LETTERS

Volatile content of lunar volcanic glasses and the presence of water in the Moon's interior

Alberto E. Saal[1], Erik H. Hauri[2], Mauro Lo Cascio[1], James A. Van Orman[3], Malcolm C. Rutherford[1] & Reid F. Cooper[1]

The Moon is generally thought to have formed and evolved through a single or a series of catastrophic heating events[1], during which most of the highly volatile elements were lost. Hydrogen, being the lightest element, is believed to have been completely lost during this period[2]. Here we make use of considerable advances in secondary ion mass spectrometry[3] to obtain improved limits on the indigenous volatile (CO_2, H_2O, F, S and Cl) contents of the most primitive basalts in the Moon—the lunar volcanic glasses. Although the pre-eruptive water content of the lunar volcanic glasses cannot be precisely constrained, numerical modelling of diffusive degassing of the very-low-Ti glasses provides a best estimate of 745 p.p.m. water, with a minimum of 260 p.p.m. at the 95 per cent confidence level. Our results indicate that, contrary to prevailing ideas, the bulk Moon might not be entirely depleted in highly volatile elements, including water. Thus, the presence of water must be considered in models constraining the Moon's formation and its thermal and chemical evolution.

Volatile elements provide insight into models of planet formation, and play a fundamental role in planetary evolution through their influence on melting[4], viscosity[5], magma crystallization[6] and volcanic eruption. An important conclusion resulting from the Apollo and Luna programmes is that the Moon is deficient in highly volatile elements relative to the Earth. This is especially the case for hydrogen, which is thought to have been completely lost during the giant collision event that generated the Moon[2].

The volatile budget of the lunar mantle can, at present, only be reconstructed from the record preserved in the mare basalts and the lunar volcanic glasses, the most primitive basalts from the Moon. Reconstructing the volatile content of the lunar mantle from basaltic melts is compromised by volatile degassing at the time the lava erupted and subsequent contamination from external sources such as low-pressure condensation following impact, solar wind implantation, and assimilation or sublimation of cometary or meteoritic material[7]. Over the past 40 years there have been considerable efforts to measure the volatile contents in these lunar samples[8–15] (see Supplementary Information). From these studies, we have reliable evidence that there is an indigenous component containing sulphur, and, to a lesser extent, chlorine, fluorine and carbon in these materials. Yet the evidence for indigenous H_2O in the lunar samples has remained elusive, consistent with the general consensus that the Moon is anhydrous.

Two main factors have limited the study of volatile abundances in lunar samples: first, most of the existing data represent bulk sample analyses, which makes it difficult to determine whether the volatile elements measured were indigenous to the glass beads or foreign (implanted, condensed or added during alteration of the sample); and second, the *in situ* analytical techniques used (Fourier transform infrared (FTIR), electron microprobe and secondary ion mass spectrometry (SIMS)) have had relatively high detection limits, particularly for H_2O and CO_2. Recent substantial advances in SIMS provide improved detection limits for H_2O, CO_2, F, S and Cl, up to two orders of magnitude lower than electron microprobe, FTIR and earlier SIMS instrumentations (see Supplementary Information). Here we report, by virtue of the new SIMS technique[3], improved limits on the indigenous volatile (CO_2, H_2O, F, S, Cl) contents of the lunar volcanic glasses and evaluate the processes controlling their variation within and between glass beads. Our results represent the first evidence for the presence of indigenous water in the lunar interior.

We investigated three main compositional groups of glasses: very-low-Ti and low-Ti glasses (sample 15427,41), and high-Ti glasses (sample 74220,864). The glassy spherules range in size from 100 to 300 μm for 74220,864 and from 200 to 400 μm with one outlier at 700 μm for 15427,41. Not all of the glass beads are completely glassy; some of them, usually the larger beads, show crystallization of either olivine (15427,41) or olivine and ilmenite (74220,864). Also, we were able to recognize four of the five compositional subgroups (A, B, C and D; group E was not sampled) of Delano's very-low-Ti glasses[16]. The major and trace element contents of the lunar volcanic glasses are consistent with previously reported data and indicate that the glasses analysed in this study represent volcanic rather than impact glasses[14,17,18] (see Supplementary Tables 1 and 2, Fig. 1 and the Methods section for detailed discussion on the analytical methods).

Essentially all volcanic glasses have carbon content (reported as CO_2) within 2σ (standard deviation) of the detection limit, with concentrations of ~6 ± 7 p.p.m. CO_2 after background correction. Carbon will not be considered further, beyond mentioning that our values give an upper limit on the concentration of carbon dissolved in the volcanic glasses. However, it is important to point out that two high-Ti glasses have 13 ± 7 and 18 ± 7 p.p.m. CO_2; if confirmed, these would be the first direct evidence for measurable dissolved carbon in any of the lunar volcanic glasses. The other volatiles, after background correction, have measurable abundances of H_2O (4–46 p.p.m.), F (4–40 p.p.m.), S (115–576 p.p.m.) and Cl (0.06–2 p.p.m.) (see Supplementary Table 1).

There are no clear correlations between the volatile contents and major and trace element contents when we consider all the compositional groups (very-low-, low- and high-Ti glasses). Yet each group has a specific range in F and S contents, suggesting differences in their initial volatile content that have not been completely erased by the degassing process acting during melt transport and eruption.

An important feature of the data is the clear correlation between H_2O, other volatile species and major elements among the very-low-Ti glasses (Fig. 1; Supplementary Figs 2, 3 and 4). These correlations indicate that H_2O in the glasses is indigenous, not a product of solar wind implantation or laboratory contamination, and support the

hypothesis that there were significant differences in the initial volatile content and/or the extent of degassing among the lunar glasses. The correlations also suggest that the major element composition of the melt may have influenced the degassing dynamics through volatile
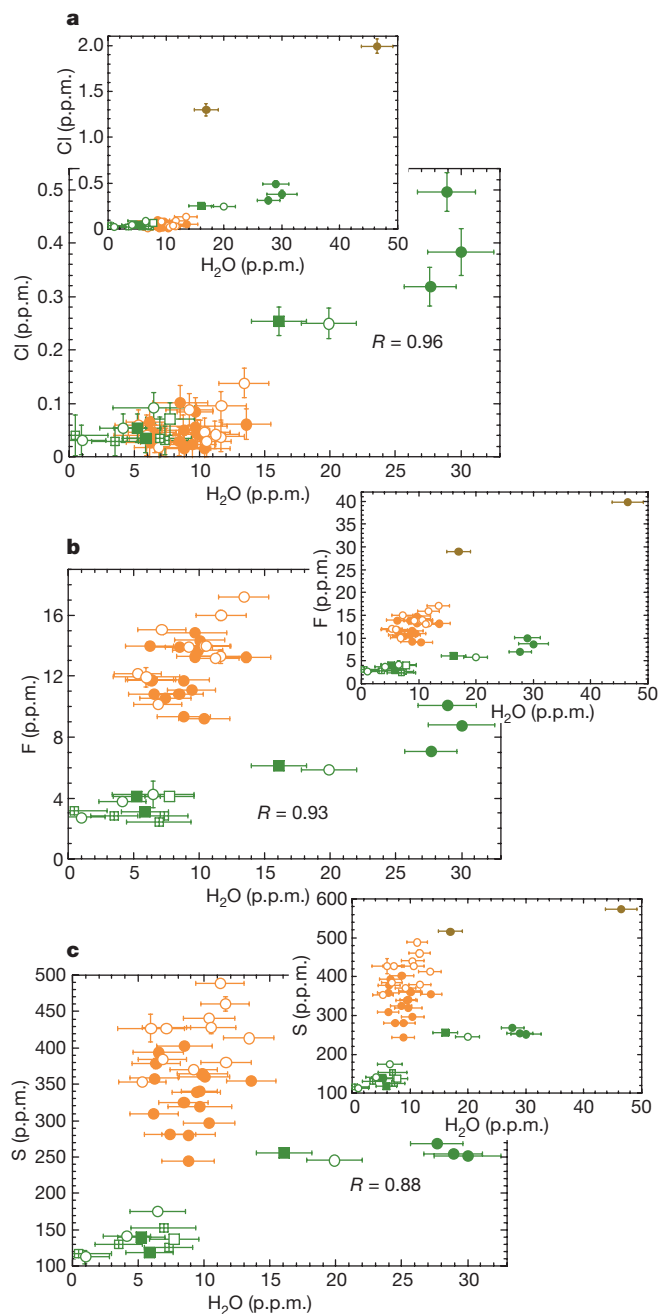

Figure 1 | Correlations between water and other volatile content in the lunar volcanic glasses. a, Chlorine; **b,** fluorine; and **c,** sulphur against H_2O content. Green symbols represent the very-low-Ti glasses: group B and C (filled circles), A (filled squares) and D (crossed open squares); partially crystallized glasses in each group are represented by open circles (group B and C) and open squares (group A). Orange filled circles represent high-Ti glasses; open orange circles indicate partially crystallized glasses. Inset shows all the glasses including the two low-Ti glasses (filled brown circles). Error bars represent standard deviation (2σ) uncertainties. Volatile contents are reported in parts per million. There are significant correlations between the volatile contents measured for the very-low-Ti glasses (see Supplementary Tables 1 and 3 and Fig. 2). Note that although the high-Ti glasses have similar Cl and H_2O contents to the very-low-Ti glasses, they have significantly higher F and S contents, suggesting different initial volatile concentrations between the different major compositional groups of glasses.

diffusion and bubble formation kinetics (see Supplementary Figs 5 and 6, and detailed discussion in the Supplementary Information on the implications of our results).

To evaluate further the hypothesis that volatiles in the lunar volcanic glasses are indigenous but affected by partial degassing during eruption, we measured radial concentration profiles for the volatiles within a single very-low-Ti glass bead (see Fig. 2; Supplementary Table 4 and the Methods section for detailed discussion on the analytical methods). Volatile contents in this bead decrease systematically from core to rim. This decrease is especially significant for H_2O, which has a concentration of ~30 p.p.m. in the centre, decreasing steadily to ~14 p.p.m. near the rim. Similar depletion towards the rim of the glass bead is observed in the data for F, Cl and S. This observation supports the hypothesis that H_2O and the other volatiles were indigenous to the glass bead but were affected by degassing during eruption. The depletion within the single glass bead reproduces essentially the same correlations between volatile elements as those defined by the volatile contents of all the very-low-Ti glasses (see Supplementary Fig. 4). This reinforces the hypothesis that degassing has been the main process affecting the primitive volatile contents of the lunar volcanic glasses.

To evaluate diffusive volatile loss from the lunar volcanic glasses during eruption, we applied a model of diffusion from a sphere with concomitant surface evaporation to the measured volatile concentration profiles within the selected glass bead[10] (Fig. 2). We emphasize that our calculations consider only volatile loss by diffusive degassing from the time of eruption until deposition, and do not consider volatile loss during the period of bubble formation and growth preceding magma fragmentation and eruption. Furthermore, we assume that there was no significant change in the distribution of volatiles within the glass beads during the period of 3.4–3.8 Gyr following their deposition[10]. This assumption is reasonable because at the average temperature on the sunlit side of the Moon (−20 to 0 °C) diffusion in the silicate glasses is negligible, and the beads have been exposed directly to the lunar surface for no more than 30 Myr (refs 19, 20). The crucial input parameters of the diffusion model are the sphere radius, the temperature of the melt during eruption, the cooling rate, the initial volatile concentrations in the glass beads, the diffusion coefficients of the volatiles within the melt, and the rates of evaporation at the surface of the melt sphere. We examined a wide range of cooling rates and times, and considered the concentration profiles for all volatiles simultaneously to determine the parameters that provided the best fit (see Supplementary Information for details on the model).

The degassing model provides excellent fits to the measured radial concentration profiles for all species simultaneously, at reasonable cooling rates and cooling times (Fig. 2). We found that cooling rates greater than $4 \, K \, s^{-1}$ did not provide acceptable fits for all volatile species (see Supplementary Fig. 7). Cooling rates of 2 to $3 \, K \, s^{-1}$ over a period of ~2 to 5 min between eruption and quenching provided the best fit to all volatile profiles together; at these conditions the glass bead loses approximately 19% S, 45% F, 57% Cl and 98% H_2O. The initial H_2O content is not precisely constrained by the modelling, but the best fit, again considering cooling rates and times that allow acceptable fits for all volatile profiles simultaneously, is obtained for an initial H_2O content of 745 p.p.m., and the H_2O content must be at least 260 p.p.m. to obtain an acceptable fit (at the 95% confidence level).

Several different origins of the lunar volatiles might be proposed. An undifferentiated lunar mantle reservoir comparatively rich in volatiles might exist at a depth greater than that of the postulated lunar magma ocean, or a less-processed cumulate that kept the primitive lunar mantle signature may have retained significant volatile elements[18]. Another possibility would be the recycling of an ilmenite-rich dense layer enriched in incompatible and volatile elements formed during the late-stage cooling and crystallization of the lunar magma ocean[21]. This process may have been responsible for the
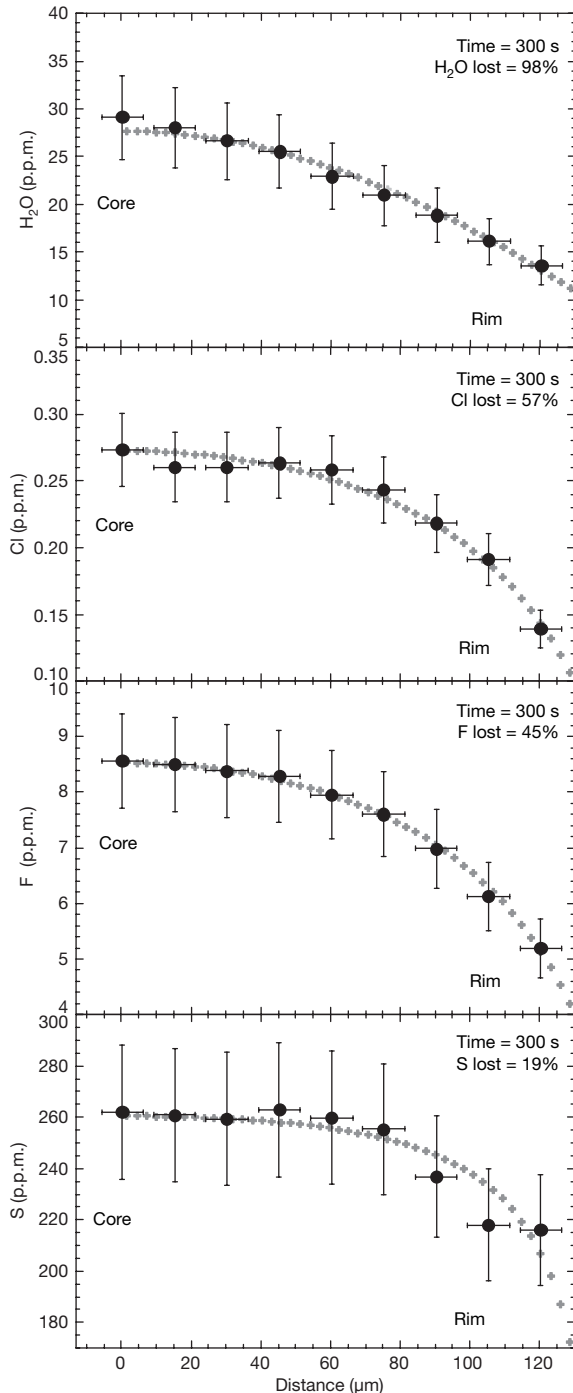
Figure 2 | Volatile concentration profiles from core to rim in a single bead of the very-low-Ti glasses. The glass used is 'Green #5' (see Supplementary Tables 1 and 4). The black filled circles represent the measured profiles, the grey filled crosses define the output data of the model describing the diffusive volatile loss from a homogeneous sphere with concomitant surface evaporation; see text for details and Supplementary Tables 4 and 5 (Case 1) for model parameters. Error bars represent standard deviation (2σ) uncertainties, and the size of the rastered ion beam. Volatile contents are in parts per million. To avoid any possible influence of ions implanted by solar wind, we did not analyse the outermost rim of the glass bead; the measured concentration profiles stop 18 μm before reaching the rim of the bead. The sharp decrease in volatile content from core to rim for H_2O, Cl, F and S suggests that the volatile contents are indigenous to the Moon and were affected by degassing during magma eruption. As expected, H_2O has the largest observed variation from core to rim, followed by Cl, F and S, indicating progressively less degassing for those elements, respectively.

re-fertilization of volatile elements into the source of the volcanic glasses.

Previous hypotheses suggest that the volatile elements either survived or were accreted after the giant impact event that probably led to the formation of the Moon. Pahlevan and Stevenson[22] suggested that the proto-Earth (having significant amounts of water) and proto-lunar disk would have diffusively equilibrated after the giant impact, and that the volatile depletion of the Moon may be explained by hydrodynamic escape from the proto-lunar disk driven by an outflow of hydrogen previously accreted to the Earth. Our results suggest either that hydrodynamic escape was not complete or that a significant amount of water was accreted to the Earth–Moon system immediately after the giant impact[23,24]. The existence of zircons on the Earth that are as old as 4,325 Myr and have oxygen isotopes of 6.5‰ provides evidence for the presence of liquid water near the Earth's surface within ~230 Myr of the Earth's accretion[25–27]. This observation strongly suggests that either the Earth–Moon system retained significant amounts of water after the giant impact, or that volatile-rich material accreted to both the Earth and Moon within a narrow time window after the giant impact but before 4.3 Gyr. At this point we do not have enough information to support or discard either of these hypotheses. Our results suggest that, contrary to the prevailing ideas, the bulk Moon might not be entirely depleted in highly volatile elements, and the presence of volatiles, especially water, must be included in models constraining the Moon's formation and its thermal and chemical evolution.

METHODS SUMMARY

Modelling. To evaluate diffusive volatile loss from the lunar volcanic glasses during eruption, we applied a model of diffusion from a sphere using a temperature-dependent diffusion coefficient with concomitant surface evaporation[10,28]. The equations and boundary conditions were solved numerically using a forward-time, centred-space finite-difference scheme[28] for each element independently. We selected the model outputs that minimized the sum of χ^2 for all of the volatiles together, using the optimum values of initial concentration and evaporation constant determined for each volatile at the cooling rate and cooling time of interest (see Supplementary Information)

Analytical method. The glass beads were individually selected and mounted in indium and analysed for major elements using the Cameca SX100 electron microprobe, and for trace and volatile elements using the Cameca IMS 6f and the NanoSIMS 50L (see online Methods and Supplementary Tables 1, 2 and 4)[3,29]. We measured the volatile contents by SIMS using methods recently developed for the simultaneous microanalysis of trace amounts of H_2O, CO_2, F, S and Cl in glasses and nominally anhydrous minerals[3].

Full Methods and any associated references are available in the online version of the paper at www.nature.com/nature.

1. Canup, R. M. Dynamics of lunar formation. *Annu. Rev. Astron. Astrophys.* **42,** 441–475 (2004).
2. Lucey, P. *et al.* in *New Views of the Moon. Reviews in Mineralogy and Geochemistry* Vol. 60 (eds Jolliff, B. L., Wieczorek, M. A., Shearer, C. K. & Niel, C. R.) 83–219 (Mineralogical Society of America, Chantilly, Virginia, 2006).
3. Hauri, E. H., Gaetani, G. A. & Green, T. H. Partitioning of water during melting of the Earth's upper mantle at H_2O-undersaturated conditions. *Earth Planet. Sci. Lett.* **248,** 715–734 (2006).
4. Gaetani, G. A. & Grove, T. L. The influence of water on melting of mantle peridotite. *Contrib. Mineral. Petrol.* **131,** 323–346 (1998).
5. Hirth, G. & Kohlstedt, D. Water in the oceanic upper mantle: implications for rheology, melt extraction and the evolution of the lithosphere. *Earth Planet. Sci. Lett.* **144,** 93–108 (1996).
6. Asimow, P. D. & Langmuir, C. H. The importance of water to oceanic mantle melting regimes. *Nature* **421,** 815–820 (2003).
7. Wieczorek, M. A. *et al.* in *New Views of the Moon. Reviews in Mineralogy and Geochemistry* Vol. 60 (eds Jolliff, B. L., Wieczorek, M. A., Shearer, C. K. & Niel, C. R.) 221–364 (Mineralogical Society of America, Chantilly, Virginia, 2006).
8. Epstein, S. & Taylor, H. P. The isotopic composition and concentration of water, hydrogen and carbon in some Apollo 15 and 16 soils and in the Apollo 17 orange soil. *Geochim. Cosmochim. Acta* **2,** 1559–1575 (1973).
9. Gibson, E. K. & Moore, G. W. Volatile-rich lunar soil: evidence of possible cometary impact. *Science* **179,** 69–71 (1973).
10. Fogel, R. A. & Rutherford, M. J. Magmatic volatiles in primitive lunar glasses; I, FTIR and EPMA analyses of Apollo 15 green and yellow glasses and revision of the

volate-assisted fire-fountain theory. *Geochim. Cosmochim. Acta* **59**, 201–215 (1995).

11. Goldberg, R. H., Burnett, D. S. & Tombrello, T. A. in *Proc. 6th Lunar Planet. Sci. Conf.* Vol. 2 2189–2200 (Pergamon, New York, 1975).

12. Jovanovic, S. & Reed, G. W. Jr. in *Proc. 6th Lunar Planet. Sci. Conf.* Vol. 2 1737–1751 (Pergamon, New York, 1975).

13. Gibson, E. K. Jr, Brett, R. & Andrawes, F. in *Proc. 8th Lunar Planet. Sci. Conf.* Vol. 2 1417–1428 (Pergamon, New York, 1977).

14. Delano, J. W., Hanson, B. Z. & Watson, E. B. in *Proc. 25th Lunar Planet. Sci. Conf.* 325–326 (Lunar and Planetary Institute, Houston, 1994).

15. Elkins-Tanton, L. T., Chatterjee, N. & Grove, T. L. Magmatic processes that produced lunar fire fountains. *Geophys. Res. Lett.* **30**, 20–21 (2003b).

16. Delano, J. W. in *Proc. 10th Lunar Planet. Sci. Conf.* Vol. 1 275–300 (Pergamon, New York, 1979).

17. Delano, J. W. Pristine lunar glasses; criteria, data, and implications. *J. Geophys. Res.* **91**, D201–D213 (1986).

18. Shearer, C. K. *et al.* in *New Views of the Moon. Reviews in Mineralogy and Geochemistry* Vol. 60 (eds Jolliff, B. L., Wieczorek, M. A., Shearer, C. K. & Niel, C. R.) 365–518 (Mineralogical Society of America, Chantilly, Virginia, 2006).

19. Lakatos, S., Heymann, D. & Yaniv, A. Green spherules from Apollo 15: Inferences about their origin from inert gas measurements. *The Moon* **7**, 132–148 (1973).

20. Eugster, O. *et al.* in *Proc. 8th Lunar Planet. Sci. Conf.* Vol. 2 3059–3082 (Pergamon, New York, 1977).

21. Hess, P. C. & Parmentier, E. M. A model for the thermal and chemical evolution of the Moon's interior; implications for the onset of mare volcanism. *Earth Planet. Sci. Lett.* **134**, 501–514 (1995).

22. Pahlevan, K. & Stevenson, D. J. Equilibration in the aftermath of the lunar-forming giant impact. *Earth Planet. Sci. Lett.* **262**, 438–449 (2007).

23. Bottke, W. F., Levison, H. F., Nesvorn, D. & Dones, L. Can planetesimals leftover from terrestrial planet formation produce the lunar Late Heavy Bombardment? *Icarus* **190**, 203–223 (2007).

24. Ryder, G. Mass flux in the ancient Earth–Moon system and benign implications for the origin of life on Earth. *J. Geophys. Res.* **107**, 5022, doi:10.1029/2001JE001583 (2002).

25. Cavosie, A. J., Valley, J. W., Wilde, S. A. & EIMF. Magmatic $\delta^{18}O$ in 4400–3900 Ma detrital zircons: A record of the alteration and recycling of crust in the Early Archean. *Earth Planet. Sci. Lett.* **235**, 663–681 (2005).

26. Wilde, S. A., Valley, J. W., Peck, W. H. & Graham, C. M. Evidence from detrital zircons for the existence of continental crust and oceans on the Earth 4.4 Gyr ago. *Nature* **409**, 175–178 (2001).

27. Mojzsis, S. J., Harrison, T. M. & Pidgeon, R. T. Oxygen-isotope evidence from ancient zircons for liquid water at the Earth's surface 4,300 Myr ago. *Nature* **409**, 178–181 (2001).

28. Crank, J. *The Mathematics of Diffusion* (Oxford Univ. Press, Oxford, UK, 1975).

29. Shimizu, N. & Hart, S. R. Application of the ion probe to geochemistry and cosmochemistry. *Annu. Rev. Earth Planet. Sci.* **10**, 483–526 (1982).

METHODS

The lunar glasses were mounted in indium and analysed for major elements using the Cameca SX100 electron microprobe at the Department of Geological Sciences, Brown University. We made the analyses using 15 kV accelerating voltage, 10 nA beam intensity, a 5–10 μm defocused beam and PAP correction procedures[30]. Most major elements reported have precision (2σ) of 1–1.5%, with the exception of Na_2O 20–60%, K_2O 20–80%, Cr_2O_3 ~15%, TiO_2 5–15%, P_2O_5 <100%, MnO <20%, which represents the average of the standard deviation of three to eight replicated analyses on a single glass bead. We reported Cr_2O_3, K_2O and P_2O_5 contents obtained using the Cameca 6f ion probe at DTM, Carnegie Institution of Washington. The precision for the trace elements measured by ion probe is better than 15% (2σ) and represents the average of the standard deviation of three to four replicated analyses on a single glass bead. SIMS calibrations are regressions of ion probe signals compared with known concentrations.

In this study, we plotted standard trace element (and volatile) concentrations against measured trace element (volatile)/^{30}Si ratios[3,29]. We measured the volatile contents by SIMS using a Cameca IMS 6f and the NanoSIMS 50L at DTM, Carnegie Institution of Washington, using methods recently developed for the microanalysis of trace amounts of H_2O, CO_2, F, S and Cl in glasses and nominally anhydrous minerals[3,31–33]. For the Cameca IMS 6f a typical 10-min measurement for volatile abundances is made on a singly polished specimen using a Cs^+ primary beam (~14 nA accelerated to 10 kV) with collection of negatively charged secondary ions. We used a 10-μm primary beam rastered at 25 μm, which results in a 35-μm crater. We pre-sputter for 3–5 min before analysis. During this time, we monitored secondary ion images of ^{12}C, ^{17}OH, ^{19}F ^{32}S and ^{35}Cl projected on the channel plate. This procedure helped to avoid inclusions and cracks, which appear as bright features on the projected image (especially the ^{12}C image), and dendritic crystals (dark shapes on ^{32}S image). After each beam spot had been carefully examined a field aperture was inserted to permit transmission of ions only from the central 10 μm of the 35-μm crater (that is, always 12.5 μm away from the crater edge), thus avoiding transmission of ions from the edge of the sputter crater and the surface of the sample. Counting times were 10 s for ^{12}C and 5 s for all other elements. Pressure in the ion probe sample chamber was ~6×10^{-10} torr during the analyses. The sample mount was placed in the ion probe sample chamber for ~12 h before analysis; this approach allowed the best detection limits for H_2O. Synthetic forsterite (Allied, <0.4 p.p.m. H_2O by FTIR) was used for the determination of H_2O detection limits[3,31–33]. All the lunar glasses were contained on a single sample mount together with synthetic forsterite; the H_2O detection limit on this particular sample mount was 6.4 p.p.m., as determined by five separate measurements interspersed with analyses of the lunar glasses. These measurements of synthetic forsterite yielded an average ^{16}OH count rate of 150 counts per second with 3,750 total counts per analysis and a Poisson limit on the precision of 3.2% (2σ), which is much lower than the actual reproducibility of the detection limit (~25%, 2σ). As a result, none of the analyses is limited in any way by counting statistics; the limiting factor is reproducibility of

the detection limit. Similar statistics are obtained for the other volatile elements on forsterite; detection limits for F, S and Cl are ~0.09 p.p.m., ~0.27 p.p.m. and ~0.03 p.p.m. respectively.

Calibrations for H_2O and other volatiles were verified for glasses and nominally anhydrous mineral standards before each analytical session; abundances for the other volatile elements (CO_2, F, S, Cl) were calculated from the calibrations performed on glass standards. The reported volatile concentrations of lunar glasses are obtained by simply subtracting the detection limit from the measured concentrations, and the uncertainties are calculated by propagating the errors in the detection limit and the counting statistics. After the measurement by the IMS 6f, we re-polished the sample and measured the core to rim volatile variation with the Cameca NanoSIMS 50L at DTM. We followed the same analytical method used on the Cameca 6f, with the exception that crater edge contamination was eliminated by electronic gating rather than a field aperture. A typical 15-min measurement used a Cs^+ primary beam (~3 nA accelerated to 8 kV) with collection of negatively charged secondary ions on multiple detectors. We used an 800-nm primary beam rastered at 12 × 12 μm area divided into 64 × 64 pixels with 140-μs dwell time per pixel, and an electronic gating on the central 4.5 × 4.5 μm. We pre-sputter for 6 min before analysis and collected the data on six detectors in multi-collection mode: ^{12}C-^{16}OH-^{19}F-^{30}Si-^{32}S-^{35}Cl at mass resolving power of ~6,000 (sufficient to resolve ^{16}OH from ^{17}O). Counting times were 1 s for all masses, and we collected 100 ratios (100 s total counting time). Pressure in the ion probe sample chamber was ~3×10^{-10} torr or less during the analyses. We used synthetic forsterite (Allied, <0.4 p.p.m. H_2O by FTIR) to establish the H_2O detection limit of 13 p.p.m., as determined by five separate measurements interspersed with analyses of the lunar glasses. Count rates for ^{16}OH were 540 counts s^{-1}, with 54,000 total counts per analysis and a Poisson precision limit of 0.002% (2σ), well below the uncertainty in the detection limits ($\pm$8% 2σ). The limiting factor on the precision is the reproducibility of the detection limit. The reported volatile concentrations of lunar glasses are obtained by simply subtracting the detection limit from the measured concentrations. For the uncertainties, we assigned a conservative 15% (2σ) for H_2O and 10% (2σ) for F, S and Cl on all the measured concentration profiles, which represent the higher uncertainty calculated by propagating the errors in the detection limit and the counting statistics obtained with the NanoSIMS.

30. Pouchou, J.-L. & Pichoir, F. in *Electron Probe Quantitation* (eds Heinrich, K. F. J. & Newberry, D. E.) 31–75 (Plenum, New York, 1991).
31. Hauri, E. H. *et al.* SIMS analysis of volatiles in silicate glasses: 1. Calibration, matrix effects and comparisons with FTIR. *Chem. Geol.* **183**, 99–114 (2002).
32. Koga, K., Hauri, E. H., Hirschmann, M. & Bell, D. Hydrogen concentration analyses using SIMS and FTIR; comparison and calibration for nominally anhydrous minerals. *Geochem. Geophys. Geosyst.* **4**, doi:10.1029/2002GC000378 (2003).
33. Aubaud, C., Hauri, E. H. & Hirschmann, M. M. Hydrogen partition coefficients between nominally anhydrous minerals and basaltic melts. *Geophys. Res. Lett.* **31**, doi:10.1029/2004GL021341 (2004).

Supplementary information

Lunar magmatism, inference about the lunar mantle, and evidence for the volcanic origin of the lunar glasses

Numerous models have been formulated for the generation and evolution of the Moon. The general consensus today is that the Moon has been produced by fission from an already-differentiated Earth during collision with a Mars-sized body[1]. The impact event and subsequent accretion of the Moon produced the heat that triggered melting and the formation of a lunar magma ocean (LMO). The estimated extent of the LMO ranges from the whole Moon[2] to only the outer 500 km[3]; whether the middle and lower mantle escaped melting and differentiation remains a matter of debate[4]. The cooling and crystallization of the LMO created layered igneous cumulates and a residual melt component (urKREEP) rich in incompatible elements and probably volatiles as well[5]. Rayleigh-Taylor instability may have caused either the sinking of a late-stage dense (ilmenite-rich) layer that mixed with the earlier cumulates[6], or a full overturn of the cumulate pile[2,7].

The extent, timing and composition of lunar magmatism are fundamental pieces of information to understand the thermal and compositional evolution of the Moon's interior. Two main types of basalts, generated from partial melting of the lunar mantle, have been studied: lava flows, which are almost exclusively exposed within the impact basins (mare basalts), and their associated volcanic glass bead deposits[8]. These latter deposits occur along the margins of impact basins adjacent to the mare basalts and in association with large vents, cinder cones and sinuous rilles[9]. The interpretation of these deposits is that they formed by eruptions in which continuous gas exsolution produced fine melt droplets in the form of pyroclastic deposits in the lunar surface, similar to Hawaiian style fire-fountaning[10].

Many of the geochemical inferences about the deepest section of the Moon have been based on the studies of the lunar volcanic glasses. These glasses have higher Mg# (Mg/Mg+Fe) and lower CaO and Al_2O_3 contents than most fine-grained non-cumulate mare basalts, and therefore represent the most primitive magmas (partial melts of the mantle source erupting without significant modification from its initial composition) on

the Moon[11]. Geochemical and experimental studies indicate that the lunar volcanic glasses were generated by melting heterogeneous LMO cumulate between 300 to 520 km within the Moon[8,12-17]. Small and variable amounts of ilmenite and urKREEP component admixed with a less processed cumulate from the lowermost reaches of the cumulate pile are thought to have comprised the heterogeneous source region that produced the diverse lunar volcanic magmas, with high-Ti (commonly named "red" and "orange") and low- to very-low-Ti (named "yellow-brown" and "green" respectively) magmas as the end-members[17].

Although an impact origin has been proposed for the lunar glasses, their volcanic origin today is wholly accepted. Among the most important lines of evidence for the volcanic origin of the lunar glasses are: 1) Shock minerals and rock fragments, schlieren, and broken crystals, which are formed during impact processes, are absent[11,18,19]. 2) Endogenous euhedral olivines, crystallized before eruption, are found in some glass beads[18]. 3) The glass deposits and mare basalts are closely associated in age[20] (~3.6-3.3 Ga. versus ~3.9-3.2 Ga.) and in space[21,22]. 4) Textural and experimental work shows that the glasses have cooled at much slower cooling rates (~1-100 ^{o}C/sec) than those expected during impact processes (~1500 ^{o}C/sec)[23,24]. An environment where the glass will cool at 1-100 ^{o}C/sec requires cooling in a surrounding high temperature (volcanic) gas atmosphere at a slower cooling rate than impact-related cooling. In contrast, the high temperature period of gas existence during impact events is much too short to allow the droplets to crystallize and have the observed textures. 5) The homogeneous major and trace element compositions of the glass beads favor the hypothesis that the glass beads were volcanic in origin[11]. Delano[11] described in detail the chemical criteria to distinguish volcanic from impact glasses. 6) The enrichment of volatile elements (B, F, Na, S, Cl, Cu, Zn, Ga, Ge, Br, Ag, Cd, In, Sb, I, Au, Hg, Tl, Pb, Bi) observed on the surface of the volcanic glasses[12,25-33] and in the vesicles within the glass beads[13,34] supports the hypothesis that the condensable elements were present in the gas driving the volcanic eruption as a fire-fountain. This interpretation is reinforced by the fact that the compositions of the surface component do not resemble any single meteoritic group[12].

Synthesis of previous volatile studies of lunar samples

Volatile elements appear to have played an important role in the generation of the lunar volcanic glasses. The association of a fire-fountain style of eruption[8] with condensation and enrichment of volatile elements on the surface of the volcanic glasses[29] suggest the existence of a deep mantle source comparatively enriched in volatiles. This implies that the Moon might not be entirely depleted in highly volatile elements. A reservoir of volatile-enriched material had to be situated deep enough within the Moon to escape the loss of volatile elements that seem to have affected the outer several hundreds kilometers within the first 200-300 My of lunar history[17,19,30,35].

There have been significant efforts to measure the volatile contents in lunar samples over the past forty years. From the bulk analyses of H_2O and CO_2 for lunar volcanic glasses, previous studies[36-40] concluded that 1) the hydrogen, and in part the carbon, were produced by implantation of solar wind on the surface of the samples; 2) the measured molecular H_2O probably represented terrestrial contamination; 3) The low carbon content measured in lunar samples has been attributed to the low C content of their source, the low solubility of C in basalts at reducing conditions (f_{O2} = I-W buffer) and CO loss during degassing[41,42].

There are few reports for fluorine and chlorine in volcanic glasses, which are mostly obtained through bulk analyses or in-situ techniques[16,26-28,34,41,43-45]. Fluorine and chlorine are at least 1-2 orders of magnitude more enriched in the surface coating of the volcanic glasses compared to their interiors; F and Cl contents of glass bead interiors in most cases were below the detection limit of the techniques used. An exception are the few electron probe data showing large enrichment of Cl up to 400 ppm close to the rim of the glass bead[41,45]. Fogel and Rutherford[41] pointed out that the x-ray signal of some or all of the chlorine could be from the Cl-rich coating, but Elkins Tanton et al.[45] interpreted the variable Cl content in the glasses as evidence for multiple glass compositions erupting simultaneously, which implies variability in the initial magma composition before fragmentation.

Sulfur has been one of the best-characterized volatile elements in the lunar volcanic glasses and mare basalts[26,41,45-49]. Bulk as well as in-situ analyses indicate that 1) Mare basalts have higher S contents than those measured in volcanic glasses within the same compositional group. 2) The reported bulk sulfur content of the volcanic glasses is up to a

factor of 4 higher than the mean S abundance within the interior of the bead glasses, suggesting significant enrichment of S condensed onto the surface of the bead. 3) There is no correlation between S and Ti content of the volcanic glasses as was previously observed for the mare basalts[49,50]. 4) Olivine-hosted melt inclusions within the volcanic glasses have between 3 and 4 times higher S content than the host glass containing the olivine[46,47]. 5) Elkins Tanton et al.[45] observed variable S content in single glass beads, increasing toward their vesicle-rich rims with increasing Ni and decreasing MgO, which suggest multiple glass compositions erupting simultaneously.

The origin of the volatile elements in the lunar volcanic glasses and implications of our results

The origin, abundance and isotopic composition of volatile elements in lunar samples have been a matter of debate, especially for H_2O. Traditionally, the H_2O and H measured in lunar samples has been interpreted as produced by either terrestrial contamination or solar wind implantation in the outer amorphous layer of regolith grains[36]. There has been clear evidence of solar wind implantation of Li, H, N, C and noble gasses, implantation that for H could reach a depth of ~100 nm from the surface of the grain[51-53]. The isotopic composition of N, H and noble gasses implanted in the lunar soil suggest the presence of two end-member components: the solar wind and ”planetary” components[53-55]. Several hypotheses have been proposed for the "planetary component": 1) interaction of the SW with the Earth's upper atmosphere (ionized by the solar radiation) generating a "wind" with Earth's like isotopic composition implanted on the lunar soil[54], 2) pre-solar solids fractionated by interstellar chemistry[53] and 3) an indigenous volatile component to the Moon, outgassed into the lunar transient atmosphere, ionized, accelerated in the electromagnetic field of the solar wind, and re-implanted into the lunar soil at enough energies to cause trapping[55]. Of these three different hypotheses only the third one would suggest areas within the Moon relatively enriched in volatiles. At this point it is impossible for us to test any of these hypotheses. Thus, a fundamental question to answer is whether the reported H_2O content in the volcanic glasses is in fact H+ implanted by solar wind, or spallation processes.

Solar wind (SW) implantation is by far the major source of extra ions to the lunar soils. Several arguments can be used to show that SW implantation has not been responsible of the measured water in the lunar volcanic glasses. First, SW does not affect the inside of the bead except for the first few microns of the surface (in the case of H is less than 100 nm); namely, the H content is surface correlated. Therefore, if the water measured were produced by solar wind implantation, we would expect an inverse correlation between the H_2O content and the glass bead size. In contrast, we observed a positive correlation between H_2O content and bead size (Supplementary Information Figure 6). Second, all the work that has been done on exposure ages of the lunar volcanic glasses sample 15426 and 74220[56-62] indicates that these glasses have either not been exposed or been exposed for a very short period of time (<30 Ma) to SW. Third, considering the implantation of SW is $\sim 3 \times 10^8$ H ions per cm^2 per sec, a simple calculation assuming that all the H from SW is stopped in the sample within the first 100 nm[53], the total amount of H implanted after a ~30 Ma exposure would be ~ 1-2 ppm H (9-18 ppm H_2O) in the first 100 nm of the glass bead. Our simple calculation above represent a maximum H concentration given that the H implanted might diffuse out into vacuum, and in less proportion into to the center of the glass bead, producing concentration profiles exactly opposed to those observed (Figure 2). Thus, if we distribute the total H content implanted in the first 100 nm over the first 18 μm (position of our analysis closest to the rim of the glass) the concentration of H_2O will be <1 ppm, below the detection limit of our technique. Fourth, even though the exposure ages for the very-low- and low-Ti glasses from sample 15426 are essentially identical, their volatile contents represent the total range measured. This observation suggests the lack of relationship between the measured volatile content (including H_2O) and the exposure ages.

Spallation processes from galactic cosmic ray (GCR) exposure could potentially affect the glass bead composition, depending on the exposure time on the Moon's surface and/or the shielding (depth of sediment cover). Cosmogenic noble gasses have been used to provide a maximum exposure age (assumed the glasses were located at the Moon surface) of ~300 Ma[56-62]. However, the amount of elements produced by spallation processes is probably several orders of magnitude less than that implanted from solar

wind; the low production of cosmogenic elements is due mainly to the element cross sections on the order of milli barns. Furthermore, it is important to emphasize that the effect of GCR on glass beads of 100-400 µm will be homogeneous, and therefore it will not produce either the observed concentration profiles, or the different volatile content in the volcanic glasses collected from the same aliquot of the sample studied (e.g., very low-Ti and low-Ti glasses from sample 15426).

Based on the data obtained on the very-low Ti glasses, there are at least four important observations indicating an indigenous origin of the measured water: 1) The correlation among H_2O, Cl, F and S contents (Figure 1, and supplementary information Figure 2), 2) the relationship between the volatile content and the major elements (Supplementary Information Table 3, Figures 3 and 5), 3) the concentration profiles in a single glass bead (Figure 2, Supplementary Information Tables 1), and 4) the concentration profiles in a single glass bead reproducing essentially the same correlations between volatile elements as those defined by the volatile contents of all the very-low-Ti glasses (Supplementary Information Tables 1 and 4 and Figure 4). These observations cannot be re-produced by solar wind implantation, spallation processes, or laboratory contamination.

The specific range in F and S contents for each major compositional group (very-low, low- and high-Ti glasses; see Supplementrary Information Figure 2c) and the clear correlation between H_2O, other volatile species, and major elements among the very-low-Ti glasses (Figure 1; Supplementary Information Figures 2, 3 and 4) would require at least one, or possibly both, of the following explanations: A) the pre-eruptive magmatic volatile content was distinct between the different major compositional groups (source difference), which in the case of the very-low-Ti glasses suggests multiple melt compositions erupting simultaneously[45]; and/or B) the extent of degassing and eruption was different between the distinct major compositional groups of glass beads. For example, the different glass groups may have had different eruptive styles and thus different cooling histories, or the major element composition of the glasses may have had a direct influence on the degassing kinetics.

The lack of correlations between the volatile and major and trace element contents among the different major compositional groups (very-low, low- and high-Ti glasses)

supports the proposition that the main process affecting the volatile concentrations of the glass beads is degassing. The specific range in F and S for each major compositional group perhaps indicates that F and S were less affected by degassing than H_2O, C, and Cl, consistent with their lower diffusivities. Therefore, F and S may have preserved actual differences in the source of the different compositional group of lunar glasses while the other volatiles did not.

The relationships between volatile and major elements among the very-low-Ti glasses suggest that the glass major element compositions may have had a direct influence on the degassing kinetics. The major element composition of a melt influences its structure and properties. We used the number of non-bridging oxygens per tetrahedrally-coordinated cation (NBO/T), calculated based on the melt stoichiometry, to quantify the melt structure of the lunar volcanic glasses. The calculated NBO/T values define a clear negative correlation with the volatile content of the lunar volcanic glasses (see Supplementary Information Figure 5). H_2O and Cl, the two fastest diffusing species, define single inverse trends versus NBO/T for all major compositional groups suggesting that degassing processes overwhelmed the initial difference (if present) in H_2O and Cl contents between these groups of glasses. Such observations suggest that most of the H_2O and Cl variation might be control by degassing processes. In contrast F and S, the two slowest diffusing species, define two trends versus NBO/T; very-low-Ti and high-Ti glasses have different S and F contents at the same NBO/T, suggesting that degassing process did not overwhelmed the initial difference in S and F concentrations between the major compositional groups. The low-Ti glasses have the lowest NBO/T and highest volatile contents, and it is impossible to determine whether their volatile concentrations are due to degassing or primitive volatile composition, or both. Several melt properties relevant to degassing are strongly correlated with NBO/T in the appropriate direction to explain the observed negative correlation with volatile contents. Melts with high NBO/T have low viscosity[63] and improved volatile diffusion and bubble formation kinetics, which enhance degassing dynamics both directly and through their influence on eruption style.

Model of diffuse volatile loss with concomitant surface evaporation

To evaluate diffusive volatile loss from the lunar volcanic glasses during eruption we applied a model of diffusion from a sphere using a temperature-dependent diffusion coefficient with concomitant surface evaporation[64,65], following the approach previously presented by Fogel and Rutherford[41]. Rather than using the analytical solutions from Fogel and Rutherford[41], the equations and boundary conditions were solved numerically using a forward-time, centered-space finite-difference scheme[64] for each element independently. The crucial input parameters of the diffusion model are: 1) the sphere radius, 2) the diffusion coefficient and activation energies of the volatiles within the melt, 3) the initial melt temperature, 4) the cooling rate, 5) the time available for diffusion (time from eruption until quenching), 6) the initial volatile concentration in the glass, and 7) the rate of evaporation at the surface of the melt sphere (which may be different for each volatile species).

We applied a simple approach to determine the input parameters. We measured the sphere radius and assumed a melt temperature of 1450 $^\circ$C. The very-low Ti glasses have a range of liquidus temperatures 1405 to 1448 $^\circ$C depending on their variable major element compositions[63]. We used the highest temperature reported for the green glasses because the most likely scenario is that the glasses erupted at temperature slightly higher than those of their liquidus. This assumption is supported by the large proportion of completely glassy beads in the sample and because the compositional trends indicate assimilation rather than crystal fractionation[16]. We used the same diffusion coefficients and activation energies as those reported in Fogel and Rutherford[41]. The exception was the activation energy for S, which is unknown; we used the activation energy for oxygen[66] as a proxy, which is reasonable since S appears to diffuse as S^{2-} rather than sulfate at low f_{O2}[67] (see Supplementary Information Table 5). The consensus is that the volcanic glasses represent melt droplets erupted into a gas cloud rather than vacuum with cooling rate (1-100 $^\circ$C/sec) as reported by all experimental work[23,24,68,69]. The cooling rates from 1 to 100 $^\circ$C/sec bracket critical cooling rates determined experimentally for the very low-Ti[23] and the high-Ti[24] glasses, respectively. The range in time from eruption until melt quenching was estimated based on the size of the dark mantle deposits (pyroclastic deposits) obtained from remote sensing data. The radial distance from the vents defined by the dark mantle deposit ranges from a few to hundreds of kilometers

(350 km from the vent is a maximum)[10]. Assuming ballistic transport at an angle of 45°, which produces the maximum distance, the time of flight ranges from ~30 to 600 seconds for deposits with radial distance from the vent less than 1 to 350 km. Finally, given that the glass transition temperature is 883 °C for the very low-Ti[23] and 938 °C for the high-Ti[24] glasses, we consider 850 °C the lower limit for running the diffusion model. The glass transition temperature gives a constraint on the maximum time to the melt quench. For example, if the initial temperature of the melt is 1450 °C and the cooling rate of 1 °C/sec, the time to quench (namely, the time at which the melt reaches the glass transition of 850 °C) will be 600 sec.

We used the parameter space described above to constrain the initial volatile concentrations and rates of evaporation that provide the best model fit to the measured volatile concentration profiles. We considered a range in cooling rates and time for the melt to quench, and for each volatile species allowed the initial concentrations and evaporation rate constant to vary to achieve the best fit (minimum χ^2 value) to the concentration profiles measured in the glass bead. We selected the model outputs that minimized the sum of χ^2 for all of the volatiles together, using the optimum values of initial concentration and evaporation constant determined for each volatile at the cooling rate and cooling time of interest. We found that: 1) the cooling rates had to be quite low, slower than 5 °C/sec; it is important to note that our estimate of the cooling rates is completely independent of the experimental work, and therefore, it is an independent confirmation that the cooling rate for the green glasses probably was as low as determined by Arndt et al.[23]. 2) the rates of evaporation had to be quite low, within the range 10^{-6} to 10^{-8} m/sec; and 3) the initial concentration for water was unexpectedly high. For example, the three model outputs that best fitted the data were found at 1 °C/sec and 600 sec time to quench, 2 °C/sec and 300 sec, and 3 °C/sec and 120 sec., with corresponding initial H_2O content of 15,000, 745 and 1,050 ppm, respectively. Models with a large range of initial H_2O contents are able to fit the measured profile well provided that there is a corresponding variation of the evaporation constant (e.g. a high initial H_2O concentration requires relatively rapid evaporation). Within the 95% confidence interval (in the linear approximation, and assuming a normal distribution of

errors in the fit parameters), adequate fits to the data can be obtained for initial H_2O concentrations between 260 ppm and 15,000 ppm.

Because the model with 600 sec time to quench (time of flight) with 1 ^{o}C/sec cooling rate describes an absolute end-member scenario, and it seems unreasonable to assume that the rate of cooling be linear for such a long duration, we did not consider the output of that model any further. The other two models, with time to quench of 300 and 120 sec with linear cooling rate at 2 ^{o}C/sec and 3 ^{o}C/sec, respectively, were considered more reasonable and are thus considered in our conclusions (See Supplementary Information Table 5). Figure 2 of the manuscript presents one example (300 sec, at 2 ^{o}C/sec) of the input and output data for the diffusive degassing model that best fit the measured volatile concentration profiles.

It is important to note that in Table 5 the radius of the glass bead is 138 μm, but in Figure 2 only shows the measured concentrations up to 120 μm from the center of the bead; our measurements stop 18 μm before reaching the rim. We did not measure the volatile content close to the rim of the glass bead in an attempt to avoid the effect of the surface correlated elements either deposited during the gas condensation, or implantated by solar wind. We model the concentration profile of the inner 120 μm and we estimated the volatile concentration at the rim (e.g., water is ~10 ppm at 138μm) from the output of the model.

Our model suggests that the enrichment of all the volatile elements (CO_2, H_2O, F, S, Cl) in the fumarolic gas not only influenced the cooling rate, but may have also affected the extent of degassing of the volatiles from the melt sphere. The non-zero concentration of volatiles at the rim of the glass bead calculated from the model (Figure 2) and the composition of the surface correlated elements[29] imply that the gas atmosphere was enriched in those volatile elements.

In our model we did not consider re-heating conditions during the depositional period, covering 3.4-3.8 Ga. Arndt et al.[23] presented evidence that no reheating occurred during or after eruption, supporting this assumption; they demonstrated that the characteristic textures experimentally produced by re-heating the glass spherules are absent in the natural glass beads.

Finally, although conditions invoking a short time to quench or very fast cooling rates would be able to reproduce the concentration profile for H_2O, given its fast diffusivity, such conditions will not reproduce the profiles for F and S due to their lower diffusivities (see Supplementary Information Figure 7). Thus, minimizing the fit to all the volatiles gives a stronger constraint to the conditions of degassing and the initial concentrations of the glass beads than matching the H_2O profile alone.

Table Captions

Table 1: Major element and volatile composition of the lunar volcanic glasses from Apollo 15 and 17 samples. The asterisk in Cr_2O_3, K_2O and P_2O_5 contents indicates that the values reported were obtained using the Cameca 6f ion probe at DTM. The column labeled "Type" indicates the different compositional sub-groups within the very-low-Ti glasses (A to D)[70]. The column labeled "Glass/Crystal" indicates which bead has partial crystallization ("Y") or is completely glassy ("N"). "Average axis" indicates the average diameter of the glass beads. NBO/T represents the number of non-bridging oxygen per tetrahedrally-coordinated cation used to quantify the melt structure. The precision for major elements reported in the table represents the average of the standard deviation (2σ) of replicated analysis (3-4 for Cr_2O_3, K_2O and P_2O_5 using the 6f SIMS, and 3-8 for major elements using the electron probe). Meanwhile, the precision for the volatile elements is reported for individual analyses and represents (2σ) uncertainties calculated by propagating the errors in the detection limit and the counting statistics. CO_2 values after background correction are within 2σ standard deviation of the detection limit, with an average concentration of $\sim 3 \pm 7$ ppm.

Table 2: Average trace element compositions of the lunar volcanic glasses. The trace elements of the glasses were determined using the Cameca 6f ion probe at DTM. The precision reported in the table represents the average of the standard deviation (2σ) of replicated analysis (3 to 4). For the very-low-Ti glasses we grouped types B with C, and A with D given their very similar trace element contents. REE values in gray italic were calculated by interpolating the values with neighboring elements in the primitive mantle normalized diagram to obtain smooth patterns.

Table 3: Correlation matrix between the volatiles contents measured in the very-low-Ti glasses.

Table 4: Volatile concentration profiles for a single glass bead of the very-low-Ti glasses. We report here volatile concentration variation from core to rim in a single bead of the very-low-Ti glass "Green # 5" in Table 1. For the uncertainties, we assigned a conservative 15% (2σ) for H_2O and 10% (2σ) for F, S and Cl on all the measured concentration profiles, which represent the higher uncertainty calculated by propagating the errors in the detection limit and the counting statistics obtained with the NanoSIMS.

Table 5: Model parameters used for modeling the diffusive volatile lost from a sphere with concomitant surface evaporation. For the calculation of the diffusion coefficients we use pre-exponential and activation energies reported in Watson et al 1982 (1)[71], Zhang and Stolper 1991 (2)[72], Watson and Bender 1980(3)[73], Dingwell and Scarfe 1984(4)[74], Delano et al. 1994(5)[50]. For S, we used the activation energy for oxygen[66] as a proxy, which is reasonable since S appears to diffuse as S^{2-} rather than sulfate at low f_{O2}[67]. The factor α represents the linear rate of evaporation (in m/sec) and describes the efficiency with which a molecule evaporates from the surface of the glass bead. We present two cases that best fit the measured volatile concentration profiles. See Figure 2 of the manuscript to evaluate the fitting of the model (Case 1) to the concentration profiles.

Figure Captions

Figure 1: Primitive mantle normalized diagram of the average trace element composition of the lunar volcanic glasses. Open symbols indicate concentrations of rare earth elements (REE) using interpolation of measured values for adjacent REE. Primitive mantle values from McDonough and Sun (1995)[75].

Figure 2: Cl-F (a) Cl-S (b) and S-F (c) in the lunar volcanic glasses. The very-low-Ti glasses are green symbols: group C and B (filled circle), A (filled square) and D

(crossed open square); partially crystallized glasses in each group are represented by open circle (group C and B) and open square (group A) symbols. Orange filled circles represent high-Ti glasses; open orange circles indicate partially crystallized glasses. Inset shows all the glasses including the two low-Ti glasses (filled brown circles). There are significant correlations (R) between the volatile contents measured for the very-low-Ti glasses; the numbers associated with R indicate the correlation coefficients (see Supplementary Table 3). Error bars represent (2σ) uncertainties calculated by propagating the standard deviation of replicated analysis in the detection limit and the counting statistics. Note that although the high-Ti glasses have similar Cl and H_2O contents to the very-low-Ti glasses, they have significantly higher F and S contents suggesting different initial volatile concentrations between the different major compositional groups of glasses. Furthermore, it is interesting to note that the glass with the highest volatile contents (low-Ti glass) has S/F ratio similar to that ratio in the Earth's primitive mantle[75] ~10, while the F/Cl ratio is one order of magnitude higher probably due to the more significant degassing of Cl.

Figure 3: H_2O, Cl, F, S and Al_2O_3/MgO versus Al_2O_3/FeO in the very-low-Ti glasses. Al_2O_3/MgO versus Al_2O_3/FeO indicates the different compositional sub-groups within the very-low-Ti glasses[70]. Error bars represent (2σ) uncertainties calculated by propagating the standard deviation of replicated analysis in the detection limit and the counting statistics. All other figures demonstrate that these different compositional sub-groups have different volatiles contents. Symbols are as in Supplementary Information Figure 2.

Figure 4: Correlation between volatile elements in the very-low-Ti glasses. All the panels in the figure show the volatile content of the individual glass beads plotted together with the volatile concentration profiles from core to rim in a single glass bead "Green # 5" (see Supplementary Information Tables 1 and 4). Error bars represent (2σ) uncertainties calculated by propagating the standard deviation of replicated analysis in the detection limit and the counting statistics. The similar trends defined by the volatile composition of individual beads to those defined by the concentration profiles in a

single bead supports the hypothesis that degassing has been the main process affecting the volatile contents of the lunar volcanic glasses. The red open squares represent the concentration profiles in a single glass bead; the other symbols are the same as in Supplementary Information Figure 2.

Figure 5: Number of non-bridging oxygen per tetrahedrally-coordinated cation (NBO/T) versus volatile contents of the lunar volcanic glasses. Error bars represent (2σ) uncertainties calculated by propagating the standard deviation of replicated analysis in the detection limit and the counting statistics. The calculated NBO/T values negatively correlate with the volatile contents of the lunar glasses indicating that the melt composition (structure) affected the degassing dynamics of volatile elements. This negative correlation is also observable when we only consider the very-low-Ti glasses. Note the different content in S and F (which were less affected by degassing than H_2O and Cl) between the different major compositional groups of volcanic glasses, suggesting distinct initial (source composition) S and F contents. Symbols as in Supplementary Information Figure 2.

Figure 6: H_2O content versus bead size of all lunar volcanic glasses studied. This figure only considers the beads that are completely glassy. Error bars represent (2σ) uncertainties calculated by propagating the standard deviation of replicated analysis in the detection limit and the counting statistics, and replicated measurements of the bead size. Because H implanted by solar wind is surface correlated, if the water measured in the glasses were due to solar wind implantation, we would expect a negative correlation between the H_2O content and the bead size. The fact that we see a positive trend suggests that the variation was most likely controlled by degassing processes. Symbols as in Supplementary Information Figure 2.

Figure 7: Comparison of the model's output for H_2O, Cl, F and S using cooling rates 10 $^{\circ}$C/sec and time to quench of 60 sec. (in red) with: 1) the model's output presented in the manuscript (cooling rate 2 $^{\circ}$C/sec and time to quench of 300 sec; in grey), and 2) the measured concentration profiles for H_2O, Cl, F and S. Error bars represent (2σ)

uncertainties calculated by propagating the standard deviation of replicated analysis in the detection limit and the counting statistics, and size of the rastered ion beam. For each pair of cooling rate and time to quench, we search for the initial concentration and surface of evaporation coefficient for H_2O, Cl, F and S that will maximize the fit to the profile data for each volatile. Although the H_2O profile can be matched by both pairs of cooling rate and times to quench (suggesting different initial concentrations of H_2O : 70 versus 745 ppm respectively), the F and S profiles are not well matched by the model with the fast cooling rates (red curve) giving a higher sum of the $\chi 2$ when fitting all the volatiles together. Thus, maximizing the fit to all the volatiles gives a stronger constraint on the conditions of degassing and the initial volatile content of the glass beads than matching the H_2O profile alone.

References

1. Canup, R. M. Dynamics of Lunar Formation. *Annu. Rev. Astron. Astrophys.* **42,** 441-475 (2004).

2. Hess, P. C. & Parmentier, E. M., A model for the thermal and chemical evolution of the Moon's interior; implications for the onset of mare volcanism. *Earth Planet. Sci. Lett.* **134,** 3-4, 501-514. (1995).

3. Hood, L. L. & Zuber, M. T. Recent refinements in geophysical constraints on lunar origin and evolution. *In Origin of the Earth and Moon* (eds. Canup, R. M. & Righter, K.) 397-409 (Univ. Arizona Press, Tucson. 2000).

4. Wieczorek, M. A., & 15 other authors, The constitution and structure of the lunar interior. *In New Views of the Moon* Reviews in Mineralogy & Geochemistry (eds. Jolliff, B. L., Wieczorek, M. A., Shearer, C. K. & Niel, C. R). Vol. 60 221-364 (Mineralogical Society of America, Chantilly, Virginia, 2006).

5. Warren, P. H., The magma ocean concept and lunar evolution. *Annu. Rev. Earth Planet. Sci.* **13,** 201-240 (1985).

6. Ringwood, A. E. & Kesson, S. E., A dynamic model for mare basalt petrogenesis. *In Petrogenetic studies of mare and highland rocks.* (eds. Merrill, R. B., Morris, R. V., Rhodes, J. M. & Usselman, T. M.). *Proceedings 7th Lunar Planet. Sc. Conf.,* Vol. **2,** 1697-1722 (1976).

7. Spera, F. J., Lunar magma transport phenomena. *In Mare volcanism and basalt petrogenesis* (eds. Faure, G., Hess, P. C. & Taylor, S. R.). *Geochimica et Cosmochimica Acta* **56,** 6, 2253-2256 (1992).

8. Shearer C.K. & other 15 authors, Thermal and magmatic evolution of the Moon. *In New Views of the Moon* Reviews in Mineralogy & Geochemistry (eds. Jolliff, B. L.,

Wieczorek, M. A., Shearer, C. K. & Niel, C. R). Vol. 60, 365-518 (Mineralogical Society of America, Chantilly, Virginia, 2006).

9. Head, J. W., Lunar volcanism in space and time. *Rev. Geophys. Space Phys.* **14,** 265-300 (1976)

10. Wilson L. & Head, J. W., Deep generation of magmatic gas on the Moon and implications for pyroclastic eruptions. *Geophys. Res. Lett.* **30,** doi:10.1029 /2002GL016082, (2003).

11. Delano, J. W., Pristine lunar glasses; criteria, data, and implications. *In Proceedings of the 16th Lunar Planet. Sc. Conf.*; (eds. Ryder, G. & Schubert, G.). *J. Geophys. Res.* B. **91,** 4, D201-D213 (1986).

12. Delano, J. W., Chemistry and liquidus phase relations of Apollo 15 red glass; implications for the deep lunar interior. *In Igneous processes and remote sensing*. (eds. Criswell, P. R. & Merrill, R. B.). *Proceedings of the 11th Lunar and Planet. Sc. Conf.* Vol. **1,** 251-288 (1980).

13. Delano, J. W. & Lindsley, D. H. Mare glasses from Apollo 17; constraints on the Moon's bulk composition. *In Proceedings of the 14th Lunar and Planet. Sc. Conf.* Part 1. (eds. Boynton, W. V. & Schubert, G.). *J. Geophys. Res.* B. **88,** Suppl. 3-16 (1983).

14. Longhi, J. Petrogenesis of picritic mare magmas: Constraints on the extent of early lunar differentiation. *Geochim. Cosmochim. Acta* **70,** 5919–5934 (2006).

15. Elkins-Tanton, L. T., Fernandez, V. A., Delano, J. W. & Grove, T. L., Origin of lunar ultramafic green glasses: Constraints from phase equilibrium studies. *Geochim. Cosmochim. Acta* **64,** 2339-2350 (2000).

16. Elkins-Tanton, L. T., Chatterjee, N. & Grove, T. L., Experimental and petrological constraints on lunar differentiation from the Apollo 15 green picritic glasses. *Meteor. Planet. Sc.* **38,** 4, 515-527 (2003).

17. Shearer, C. K. & Papike, J. J., Basaltic magmatism on the Moon; a perspective from volcanic picritic glass beads. *Geochim. Cosmochim. Acta* **57,** 19, 4785-4812 (1993).

18. Heiken, G. H., McKay, D. S. & Brown, R. W., Lunar deposits of possible pyroclastic origin. *Geochim. Cosmochim. Acta* **38,** 11, 1703-1718 (1974).

19. Delano, J. W. & Livi, K., Lunar volcanic glasses and their constraints on mare petrogenesis. *Geochim. Cosmochim. Acta*. **45,** 11, 2137-2149 (1981).

20. Snyder, G. A., Brog, L. E. Nyquist, L. E. & Taylor, L. A. Chronology and isotopic constraints on lunar origin and evolution. *In Origin of the Earth and Moon* (eds. Canup, R. M. & Righter, K.) 361-396 (University of Arizona Press, 2000)

21. Hiesinger, H. & Head, J. W., An Introduction and Overview. *In New Views of the Moon* Reviews in Mineralogy & Geochemistry (eds. Jolliff, B. L., Wieczorek, M. A., Shearer, C. K. & Niel, C. R). Vol. 60 1-81 (Mineralogical Society of America, Chantilly, Virginia, 2006).

22. Head, J. W., Wilson, L. & Weitz, C. M. Dark ring in southwestern Orientale Basin: Origin as a single pyroclastic eruption. *J. Geophys. Res.* **107,** (E1), doi:10.1029/2000JE001438, (2002).

23. Arndt, J., Engelhardt, W. V., Gonzalez-Cabeza, I., & Meier, B., Formation of Apollo 15 green glass beads. *In Proceedings of the 15th Lunar Planet. Sc. Conf.* (Houston); *J. Geophys. Res.* Suppl. 89, C225-C232. (1984).

24. Arndt J. & Engelhardt W. V. Formation of Apollo 17 orange and black glasses. *In Proceedings of the 17th Lunar Planet. Sc. Conf.* (Houston); *J. Geophys. Res.* Suppl. 92, E372-E376 (1987).

25. Butler, P. Jr., Recognition of lunar glass droplets produced directly from endogenous liquids; the evidence from S-Zn coatings. *In Lunar and Planetary Surfaces* (eds. Merrill, R. B.). *Proceedings of the 9th Lunar Planet. Sc. Conf.*, Vol. 2, 1459-1471 (1978).

26. Butler, P. Jr. & Meyer, C. Jr. Sulfur prevails in coatings on glass droplets; Apollo 15 green and brown glasses and Apollo 17 orange and black (devitrified) glasses. *In Petrogenetic studies of mare and highland rocks.* (eds. Merrill, R. B., Morris, R. V., Rhodes, J. M. & Usselman, T. M.). *Proceedings 7th Lunar Planet. Sc. Conf.,* Vol. **2,** 1561-1581 (1976).

27. Chou, C. L., Boynton, W. V., Sundberg, L. L. & Wasson, J.T., Volatiles on the surface of Apollo 15 green glass and trace-element distributions among Apollo 15 soils. *In Chemical and isotopic studies* (eds. Merrill, R. B., Hubbard, N. J., Mendell, W. W. & Williams, R. J.) *Proceedings 6th Lunar Planet. Sc. Conf.,* Vol. **2,** 1701-1727 (1975).

28. Meyer, C. Jr., McKay, D.S., Anderson, D.H. and Butler, P. Jr. The source of sublimates on the Apollo 15 green and Apollo 17 orange glass samples. *In Chemical and isotopic studies* (eds. Merrill, R. B., Hubbard, N. J., Mendell, W. W. & Williams, R. J.) *Proceedings 6th Lunar Planet. Sc. Conf.,* Vol. **2,** 1673-1699 (1975).

29. Wasson, J. T., Boynton, W. V., Kallemeyn, G. W., Sundberg, L. L. & Wai, C. M., Volatile compounds released during lunar lava fountaining. *In Petrogenetic studies of mare and highland rocks.* (eds. Merrill, R. B., Morris, R. V., Rhodes, J. M. & Usselman, T. M.). *Proceedings 7th Lunar Planet. Sc. Conf.,* Vol. **2,** 1583-1595 (1976).

30. Delano, J. W., The early evolution of the moon as inferred from mare basaltic liquids. *In Pristine Lunar Highlands Rocks and the Early Evolution of the Moon.* (eds. Longhi, J., Ryder, G.). Lunar and Planetary Institute, Technical Report 83-02, pp. 36-43. (Lunar and Planetary Institute, Houston, 1983).

31. Krähenbühl U. Distribution of volatile and non volatile elements in grain-size fractions of Apollo 17 drive tube 74001/2. *In Igneous processes and remote sensing.* (eds. Criswell, P. R. & Merrill, R. B.). *Proceedings of the 11th Lunar and Planet. Sc. Conf.* Vol. 2, 1551-1564 (1980).

32. Morgan, J. W., & Wandless, G. A., Surface correlated trace elements in 15426 lunar glasses. *Proceedings of the 15th Lunar and Planet. Sc. Conf.*, 562-563 (1984).

33. Clanton, U. S., McKay, D. S., Waits G. & Fuhrman, R., Sublimate morphology on 74001 and 74002 orange and black glassy droplets *In Lunar and Planetary Surfaces*

(eds. Merrill, R. B.). *Proceedings of the 9th Lunar Planet. Sc. Conf.*, Vol. 2, 1945-1957 (1978).

34. Goldberg, R. H., Burnett, D. S. & Tombrello, T. A., Fluorine surface films on lunar samples: Evidence for both lunar and terrestrial origin. *In Proceedings of the 6th Lunar Planet. Sc. Conf.* (Houston) 2189-2200, (1975).

35. Clive, R. N. Interior of the Moon: The presence of garnet in the primitive deep lunar mantle. *J. Geophys. Res.* Vol. **106,** E11, 27,865-27,885 (2001).

36. Epstein, S. & Taylor, H. P., The isotopic composition and concentration of water, hydrogen and carbon in some Apollo 15 and 16 soils and in the Apollo 17 orange soil . *In Proceedings of the 4th Lunar and Planet. Sc. Conf.* (suppl. 4), *Geochim. Cosmochim. Acta* Vol 2, 1559-1575 (1973).

37. Friedman, I., Hardcastle, K. G., & Gleason J. D., Isotopic composition of carbon and hydrogen in some Apollo 14 and 15 samples. *In The Apollo 15 Lunar Samples,* 302-306. (The Lunar Science Institute, Houston, 1972).

38. Kaplan, I. R. & Petrowski, C., Carbon and Sulfur isotope studies on Apollo 12 lunar samples. *In Proceedings of the 2th Lunar and Planet. Sc. Conf.* Suppl 2, *Geochim. Cosmochim. Acta* **2,** 1397-1406 (1971).

39. Gibson, E. K. & Moore, G. W. Volatile-rich lunar soil: evidence of possible cometary impact. *Science* **179,** 69-71 (1973).

40. Gibson, E. K., Volatile elements, carbon, nitrogen, sulfur, sodium, potassium and rubidium in the lunar regolith. *Physics and Chemistry of the Earth,* **10,** 1, 1977, 57-62, (1977)

41. Fogel, R. A. & Rutherford, M. J., Magmatic volatiles in primitive lunar glasses; I, FTIR and EPMA analyses of Apollo 15 green and yellow glasses and revision of the volatile-assisted fire-fountain theory. *Geochim. Cosmochim. Acta* **59,** 1, 201-215 (1995).

42. Sato, M. The driving mechanism of lunar pyroclastic eruptions inferred from the oxygen fugacity behavior of Apollo 17 orange glass. *In Meteorites and lunar rocks* (eds. Merrill, R. B., Bogard, D. D., McKay, D. S. & Robertson, P.C.). *Proceedings of the 10th Lunar Planet. Sc. Conf.*, Vol. 1, 311-325 (1979).

43. Jovanovic, S., Jensen, K. & Reed, G. W. Jr. Trace Elements and the Evolution of Lunar Rocks. *In Petrogenetic studies of mare and highland rocks.* (eds. Merrill, R. B., Morris, R. V., Rhodes, J. M. & Usselman, T. M.). *Proceedings 7th Lunar Planet. Sc. Conf.,* Vol. 2, 437-439 (1976).

44. Jovanovic, S. & Reed, G. W. Jr., Cl and P_2O_5 systematics: Clue to early lunar magmas. *In Proceedings of the 6th Lunar Planet. Sc. Conf.* (Houston), 1737-1751 (1975).

45. Elkins-Tanton, L. T., Chatterjee, N. & Grove, T. L., Magmatic processes that produced lunar fire fountains. *Geophys. Res. Lett.*, **30,** 10, 20-1, (2003b)

46. Weitz, C. M., Rutherford, M. J., Head, J. W. III & McKay, D. S., Ascent and eruption of a lunar high-titanium magma as inferred from the petrology of the 74001/ 2 drill core. *Meteor. Planet. Sc.* **34,** 4, 527-540 (1999).

47. Klein, N. & Rutherford, M. J., Volcanic Gas Formed During Eruption of Apollo 17 Orange Glass Magma; Evidence from Glassy Melt Inclusions and Experiments. *In The 29th Annual Lunar and Planetary Science Conference*. Abstract no.1448 (Houston, TX, 1998).

48. Gibson, E. K. Jr. & Andrawes, F. F., Sulfur abundances in the 74001/74002 drive tube core from Shorty Crater, Apollo 17. *In Proceedings of the 9th Lunar Planet. Sc. Conf.*, Houston, Vol. 2., 2011-2017 (1978).

49. Gibson, E. K., Chang, S., Lennon, K., Moore, G. W., & Pearce, G. W., Sulfur abundances and distributions in mare basalts and their source magmas. *In Proceedings of the 6th Lunar Planet. Sc. Conf.*, Houston, 1287-1301 (1975).

50. Delano, J. W., Hanson, B. Z. & Watson, E. B., Abundance and diffusion of sulfur in lunar picritic magmas. *In Proceedings of the 25th Lunar Planet. Sc. Conf.*, 325-326. (Lunar and Planetary Institute, Houston. 1994).

51. Chaussidon, M. & Robert, F. Lithium nucleosynthesis in the Sun inferred from the solar-wind 7Li/6Li ratio. *Nature*, **402,** 6759, 270-273 (1999).

52. Hashizume, K., Chaussidon, M., Marty, B. & Terada, K., Protosolar Carbon Isotopic Composition: Implications for the Origin of Meteoritic Organics. *Astrophysical J.*, **600,** 480-484 (2004).

53. Hashizume K., Chaussidon M., Marty, B. & Robert F., Solar Wind Record on the Moon: Deciphering Presolar from Planetary Nitrogen. *Science*, **290,** 5494, 1142 –1145. (2000).

54. Ozima1, M., Seki, K., Terada, N. Miura, Y. N., Podosek, F. A., & Shinagawa, H., Terrestrial nitrogen and noble gases in lunar soils. *Nature,* **436,** 4, 655-659, (2005).

55. Eugster, O., Terribilini, D., Polnau, E. & Kramers J., The antiquity indicator argon-40/argon-36 for lunar surface samples calibrated by uranium-235-xenon-136 dating. *Meteor. Planet. Sc.* **36,** 1097-1115 (2001).

56. Eugster, O., Eberhardt, P., Geiss, J., Gröngler N., Jungck, M. & Mörgeli M. The cosmic-ray exposure history of Shorty Crater samples; the age of Shorty Crater. *In Proceedings of the 8th Lunar Planet. Sc. Conf.* 3059-3082 (1977).

57. Podosek, F. A. & Huneke, J. C., Argon in Apollo 15 green glass spherules (15426): 40Ar-39Ar Age and trapped argon. *Earth Planet. Sci. Lett.* **19,** 413-421 (1973).

58. Eugster, O., Gröngler N., Eberhardt, P., Geiss, J. & Keisl, W. Double drive tube 74001/2: A two-stage exposure model based on noble gases, chemical abundances and predicted production rates. *In Proceedings of the 12Bth Lunar Planet. Sc. Conf.* 541-558 (1981).

59. Lakatos, S., Heymann D. & Yaniv A., Green spherules from Apollo 15: Inferences about their origin from inert gas measurements. *In The Moon 7,* (D. Reidel Publishing Company, Holland) pp 132-148 (1973).

60. Fleischer, R. L. & Hart, H. R., Jr. Particle track record of Apollo 15 green soil and rock *Earth Planet. Sci. Lett.* **18,** (2) 357-364 (1973).

61. Spangler, R. R.; Warasila, R. & Delano, J. W., Ar-39-Ar-40 ages for the Apollo 15 green and yellow volcanic glasses. *In Proceedings of the 14th Lunar and Planet. Sc. Conf.* Part 1. *J. Geophys. Res.* **89,** B487-B497 (1984).

62. Spangler, R. R. & Delano, J. W., History of the Apollo 15 yellow impact glass and sample 15426 and 15427. *In Proceedings of the 14th Lunar and Planet. Sc. Conf.* Part 1. *J. Geophys. Res.* **89,** B478 - B486 (1984).

63. Delano, J. W., Buoyancy-driven melt segregation in the Earth's moon, I Numerical Results. *In Proceedings of the 20th Lunar Planet. Sc. Conf.* (Houston), 3-12 (1990).

64. Crank, J. The Marhematics of Diffusion. (Oxford University Press, Clarendon, Oxford, UK, 1975).

65. Dodson, M. H., Closure temperature in cooling geochronological and petrological systems. *Contrib. Mineral. Petrol.* **40,** 259-214 (1973).

66. Wendlandt, R. F., Oxygen diffusion in basalt and andesite melts: Experimental results and discussion of chemical versus tracer diffusion. *Contrib. Mineral. Petrol.* **108**, 463-471 (1991).

67. Baker, L. L. & Rutherford, M. J., Sulfur diffusion in rhyolite melts. *Contrib. Mineral. Petrol.* **123**, 335-344 (1996).

68. Fang, C. Y., Yinnon, H. & Uklmann, D. R., Cooling rates for glass containing lunar compositions. *In Proceedings of the 13th Lunar and Planet. Sc. Conf.* Part 1. *J. Geophys. Res.* **88,** A907-A911 (1983).

69. Uhlmann, D. R., Yinnon, H.& Fang, C. Y., Simplified model evaluation of cooling rates for glass-containing lunar compositions. *In Proceedings of the 12th Lunar and Planet. Sc. Conf.* Section 1, 281-288 (1982).

70. Delano, J. W., Apollo 15 green glass - Chemistry and possible origin. *Proceedings 10th Lunar Planet. Sc. Conf.*, (Houston) Vol. 1. 275-300 (New York, Pergamon Press, Inc. 1979).

71. Watson, E. B., Sneeringer M. A., & Ross, A., Diffusion of dissolved carbonate in magmas: Experimental results and applications. *Earth Planet. Sci. Lett.* **61,** 346-358 (1982).

72. Zhang, Y. & Stolper, E. M., Water diffusion in basaltic melt. *Nature* **351,** 306-309 (1991).

73. Watson, E. B. & Bender, J. F. Diffusion of cesium, samarium, strontium and chlorine in molten silicate at high temperatures and pressures. *Geol. Soc. Am.* Abstr. Progr. **12,** 545 (1980).

74. Dingwell, D. B. & Scarfe, C. M., Chemical diffusion of fluorine in jadeite melt at high pressure. *Geochim. Cosmochim. Acta* **48,** 2517-2525 (1984).

75. McDonough W.F. and Sun S.-s., The composition of the Earth., *Chem. Geol.* **120,** 223-253, (1995).

Supplementary Table 1: Major Element and Volatile Composition of the Lunar Volcanic Glasses.

Sample	SiO$_2$	Al$_2$O$_3$	TiO$_2$	Cr$_2$O$_3$*	FeO	MnO	CaO	MgO	Na$_2$O	K$_2$O*	P$_2$O$_5$*	Total	Type	Glass/Crystal	average axis (μ)	NBO/T
15427 Very-Low-Ti Glasses																
Green#1	48.45	10.80	0.565	0.668	19.23	0.294	12.72	7.32	0.129	0.015	0.022	100.21	B	Y	737.5	1.107
Green#2	44.93	7.60	0.405	0.612	20.39	0.281	8.92	16.34	0.078	0.012	0.020	99.60	A	Y	135	1.703
Green#3	48.50	10.73	0.597	0.672	19.23	0.298	13.04	6.87	0.116	0.012	0.022	100.09	B	Y	462	1.098
Green#4	45.89	7.83	0.374	0.641	19.56	0.271	8.65	16.91	0.111	0.014	0.023	100.27	A	N	221.5	1.655
Green#5	48.02	7.82	0.296	0.612	16.75	0.256	8.66	17.96	0.118	0.009	0.020	100.52	C	N	308.5	1.594
Green#6	47.90	7.93	0.317	0.612	17.35	0.271	9.09	16.67	0.105	0.009	0.020	100.27	B	Y	320.5	1.536
Green#7	45.44	7.48	0.461	0.634	20.30	0.279	8.26	17.42	0.111	0.012	0.024	100.42	D	N	266.5	1.723
Green#8	46.02	7.97	0.399	0.628	19.26	0.262	8.66	16.92	0.141	0.013	0.023	100.30	A	N	316.5	1.637
Green#9	49.36	11.74	0.682	0.586	17.95	0.280	14.06	5.07	0.146	0.013	0.024	99.91	B	Y	364	0.965
Green#10	47.30	7.96	0.354	0.620	17.53	0.272	8.60	17.61	0.079	0.012	0.025	100.36	B	N	371	1.584
Green#11	45.62	7.86	0.407	0.635	19.81	0.274	8.68	16.89	0.142	0.012	0.020	100.34	A	N	390.5	1.695
Green#12	45.38	7.69	0.421	0.633	20.22	0.278	8.41	17.07	0.123	0.013	0.021	100.26	D	N	215.5	1.699
Green#13	45.21	7.41	0.421	0.633	20.42	0.301	8.37	17.36	0.095	0.012	0.020	100.25	D	N	210	1.740
Green#14	45.88	7.68	0.403	0.633	19.75	0.251	8.74	17.00	0.150	0.012	0.020	100.53	A	N	213	1.679
Green#15	46.43	7.97	0.444	0.633	18.76	0.287	8.79	17.08	0.159	0.012	0.020	100.58	B	N	300	1.626
Green#16	45.57	7.62	0.416	0.633	20.30	0.280	8.50	17.14	0.120	0.012	0.020	100.60	D	N	220	1.707
15427 Low-Ti Glasses																
Yellow-Brown#1	42.87	8.64	3.605	0.699	21.76	0.277	8.46	12.80	0.378	0.075	0.088	99.65		N	350.5	1.496
Yellow-Brown#2	42.74	8.09	3.607	0.741	22.22	0.307	8.26	13.63	0.263	0.064	0.080	100.00		N	243.5	1.549
74220 High-Ti Glasses																
Orange#1	38.74	5.87	9.303	0.855	22.51	0.310	7.38	14.73	0.404	0.073	0.024	100.20		N	169.5	1.688
Orange#2	38.90	5.89	9.318	0.857	22.56	0.312	7.52	14.98	0.325	0.072	0.023	100.76		N	212	1.698
Orange#3	38.64	5.77	9.002	0.857	22.52	0.308	7.27	15.36	0.344	0.067	0.023	100.16		N	187	1.725
Orange#4	38.96	6.52	10.411	0.852	22.46	0.309	8.45	12.02	0.422	0.063	0.024	100.48		Y	353	1.516
Orange#5	38.95	5.80	9.241	0.857	22.86	0.279	7.39	14.96	0.338	0.063	0.023	100.75		Y	207.5	1.705
Orange#6	38.92	5.99	9.506	0.867	22.74	0.291	7.77	13.95	0.348	0.063	0.024	100.48		N	226	1.645
Orange#7	38.82	5.79	9.153	0.857	22.38	0.276	7.31	15.22	0.316	0.066	0.023	100.21		N	228	1.708
Orange#8	38.80	5.82	9.219	0.853	22.53	0.292	7.34	15.22	0.152	0.072	0.023	100.32		N	261.5	1.708
Orange#9	38.87	5.82	9.274	0.848	22.66	0.287	7.29	15.11	0.130	0.067	0.023	100.38		N	233.5	1.702
Orange#10	38.87	5.82	9.274	0.849	22.66	0.287	7.29	15.11	0.130	0.061	0.023	100.38		N	143.00	1.702
Orange#11	38.66	5.91	9.268	0.851	22.52	0.287	7.35	14.93	0.227	0.068	0.024	100.10		N	116	1.728
Orange#12	39.11	6.16	10.082	0.811	23.09	0.323	8.37	11.87	0.117	0.064	0.026	100.02		Y	235.5	1.531
Orange#13	38.86	5.84	9.140	0.851	22.56	0.300	7.41	14.89	0.352	0.071	0.024	100.30		N	162.5	1.698
Orange#14	38.87	5.85	9.161	0.846	22.74	0.318	7.46	14.86	0.250	0.074	0.025	100.46		N	111.5	1.699
Orange#15	38.68	5.77	9.103	0.850	22.58	0.306	7.23	15.26	0.357	0.067	0.023	100.24		N	209	1.723
Orange#16	38.81	5.94	9.560	0.847	22.48	0.296	7.53	14.35	0.352	0.068	0.024	100.25		Y	189.5	1.694
Orange#17	38.87	5.92	9.207	0.846	22.56	0.272	7.41	15.07	0.363	0.066	0.024	100.61		N	165.5	1.702
Orange#18	38.76	5.77	9.236	0.852	22.64	0.303	7.39	15.24	0.359	0.065	0.023	100.64		N	153.5	1.724
Orange#19	38.64	6.20	9.678	0.866	22.99	0.272	7.81	13.21	0.287	0.061	0.025	100.03		Y	239	1.610
Orange#20	38.85	5.89	9.316	0.844	22.82	0.293	7.39	15.00	0.233	0.064	0.024	100.72		Y	280	1.701
Orange#21	38.83	5.89	9.209	0.849	22.38	0.262	7.36	14.89	0.303	0.064	0.023	100.06		N	163	1.684
Orange#22	38.76	6.25	9.882	0.859	22.57	0.302	8.10	12.73	0.200	0.077	0.026	99.76		Y	299.5	1.557
Orange#23	38.49	5.81	9.209	0.850	22.39	0.283	7.44	15.00	0.263	0.063	0.023	99.83		N	139	1.708
Orange#24	38.96	6.66	10.343	0.924	22.36	0.300	8.52	11.82	0.239	0.083	0.027	100.23		Y	221.5	1.506
Orange#25	39.00	6.21	9.711	0.830	22.68	0.311	8.20	12.95	0.304	0.069	0.025	100.29		Y	165.5	1.585
Orange#26	39.21	7.02	11.197	0.751	22.39	0.313	9.36	9.26	0.344	0.074	0.027	99.95		Y	155.5	1.350
Orange#27	39.97	7.75	13.208	0.847	21.16	0.294	11.34	5.62	0.367	0.074	0.027	100.65		Y	160	1.148
Orange#28	39.25	6.54	10.558	0.847	22.90	0.292	8.57	10.90	0.322	0.074	0.024	100.27		Y	150	1.463
Error in % (2σ)	<2	<2	05-15	<10	<2	<20	<2	<2	20-60	<10	<10					

Supplementary Table 1: Major Element and Volatile Composition of the Lunar Volcanic Glasses.

Sample	CO$_2$ ppm	S.D. (2σ)	H$_2$O ppm	S.D. (2σ)	F ppm	S.D. (2σ)	S ppm	S.D. (2σ)	Cl ppm	S.D. (2σ)
15427 Very-Low-Ti Glasses										
Green#1	~DL		6.39	3.11	4.28	0.86	176.1	48.4	0.094	0.028
Green#2	~DL		7.65	1.85	4.18	0.13	138.5	3.4	0.072	0.030
Green#3	~DL		4.04	1.80	3.84	0.12	143.0	1.0	0.056	0.027
Green#4	~DL		5.14	1.78	4.18	0.13	140.6	2.0	0.055	0.027
Green#5	~DL		27.58	1.96	7.13	0.20	269.6	3.5	0.321	0.036
Green#6	~DL		19.82	2.08	5.91	0.12	246.5	2.3	0.251	0.029
Green#7	~DL		7.23	1.80	2.89	0.11	127.2	1.4	0.032	0.027
Green#8	~DL		16.01	2.11	6.20	0.13	257.4	0.4	0.256	0.027
Green#9	~DL		0.90	1.83	2.79	0.24	113.8	9.0	0.033	0.027
Green#10	~DL		28.86	2.22	10.17	0.14	255.3	0.5	0.499	0.036
Green#11	~DL		5.80	1.81	3.17	0.11	120.2	0.7	0.037	0.027
Green#12	~DL		3.45	1.82	2.90	0.12	131.5	0.7	0.030	0.026
Green#13	~DL		6.84	2.47	2.52	0.08	154.1	3.3	0.037	0.039
Green#14	~DL		1.23	2.45	2.33	0.08	133.1	2.8	0.030	0.040
Green#15	~DL		29.93	2.57	8.84	0.24	253.2	4.7	0.386	0.044
Green#16	~DL		0.42	2.47	3.22	0.13	117.9	1.7	0.042	0.038
15427 Low-Ti Glasses										
Yellow-Brown#1	~DL		46.37	2.72	39.96	0.57	575.7	2.3	2.00	0.08
Yellow-Brown#2	~DL		16.83	2.10	29.14	0.34	518.1	6.5	1.31	0.06
74220 High-Ti Glasses										
Orange#1	~DL		6.11	1.83	11.84	0.23	311.0	3.6	0.067	0.026
Orange#2	~DL		6.27	1.85	11.80	0.30	379.8	6.6	0.048	0.029
Orange#3	~DL		6.13	1.85	14.04	0.24	359.5	3.9	0.029	0.027
Orange#4	~DL		7.06	1.84	15.11	0.23	428.7	4.7	0.030	0.026
Orange#5	~DL		5.22	1.82	12.23	0.23	354.5	5.0	0.062	0.029
Orange#6	~DL		8.44	2.08	13.97	0.17	404.4	4.7	0.104	0.032
Orange#7	13.1	7.2	7.36	1.97	10.61	0.24	282.7	2.9	0.028	0.027
Orange#8	~DL		9.58	1.36	13.34	1.39	342.3	39.7	0.087	0.027
Orange#9	~DL		8.38	1.86	10.91	0.16	326.8	3.3	0.030	0.027
Orange#10	~DL		8.71	1.95	11.79	0.17	245.3	2.5	0.052	0.027
Orange#11	~DL		9.35	1.83	11.16	0.16	340.1	2.0	0.025	0.028
Orange#12	~DL		10.32	1.95	14.02	0.27	442.0	2.8	0.048	0.027
Orange#13	~DL		9.79	1.89	13.74	0.15	365.3	4.0	0.045	0.026
Orange#14	~DL		6.48	1.91	10.88	0.12	395.0	3.6	0.036	0.026
Orange#15	~DL		8.74	2.02	9.40	0.23	281.7	4.0	0.017	0.026
Orange#16	~DL		9.12	1.79	13.97	0.19	372.0	5.3	0.090	0.029
Orange#17	~DL		13.50	1.84	13.30	0.31	355.8	5.7	0.062	0.028
Orange#18	~DL		9.98	1.92	14.40	0.14	361.7	4.3	0.043	0.027
Orange#19	~DL		13.33	1.91	17.26	0.19	414.7	4.9	0.139	0.027
Orange#20	~DL		11.58	1.90	16.04	0.34	381.4	6.2	0.097	0.026
Orange#21	~DL		10.32	1.94	9.25	0.27	298.0	4.8	0.018	0.025
Orange#22	~DL		6.76	1.82	10.19	0.14	386.2	4.1	0.019	0.026
Orange#23	~DL		9.58	2.41	14.92	0.17	320.5	2.6	0.058	0.029
Orange#24	18.2	7.1	11.52	1.83	13.35	0.44	461.7	9.5	0.039	0.027
Orange#25	~DL		10.47	1.88	14.06	0.16	429.4	8.6	0.030	0.027
Orange#26	~DL		11.12	1.80	13.23	0.14	489.9	3.5	0.043	0.026
Orange#27	~DL		5.89	2.56	12.00	0.66	428.5	19.7	0.042	0.038
Orange#28	~DL		~DL		11.58	0.43	450.2	14.2	0.065	0.038

Supplementary Information Table 2: Average trace element compositions of the lunar volcanic glasses.

Average Trace Elements					
Sample	**74220**	**15427**	**15427**	**15427**	**Error in % (2s)**
Melt Type	**High-Ti**	**Low-Ti**	**Very-Low-Ti (B-C)**	**Very-Low-Ti (A-D)**	
Ba	86.65	89.91	13.17	17.01	<10
Nb	17.39	11.23	1.31	1.70	<10
K	556.40	566.67	83.13	106.25	<15
La	6.80	8.62	1.11	1.48	<15
Ce	20.82	23.99	2.99	3.74	<10
Pr	*3.60*	*3.66*	*0.44*	*0.53*	
Sr	228.50	160.94	19.00	26.23	<10
Nd	19.91	18.14	2.13	2.47	<15
Zr	197.68	164.58	17.20	22.62	<10
Hf	6.79	4.90	0.60	0.68	<15
Sm	7.10	6.06	0.68	0.83	<15
Eu	1.90	1.49	0.17	0.24	<15
Ti	60566.93	22694.51	1902.58	2425.24	<10
Gd	8.03	6.93	0.91	1.13	<15
Tb	*1.47*	*1.31*	*0.18*	*0.21*	
Dy	10.06	9.23	1.27	1.53	<15
Y	50.07	47.80	7.53	8.99	<10
Ho	*2.10*	*1.98*	*0.29*	*0.34*	
Er	5.82	5.64	0.90	1.04	<15
Tm	*0.82*	*0.80*	*0.14*	*0.16*	
Yb	4.83	4.69	0.92	1.06	<15
Lu	*0.70*	*0.69*	*0.15*	*0.17*	

Supplementary Information Table 3: Correlation Matrix Between the Volatile Contents Measured for the Very-Low-Ti Glasses

	H$_2$O ppm	F ppm	S ppm	Cl ppm
H$_2$O ppm	1			
F ppm	0.9333	1		
S ppm	0.8845	0.8683	1	
Cl ppm	0.956	0.9797	0.8897	1

Supplementary Information Table 4: Volatile Concentration Profiles for a Single Glass Bead #5

Distance μ	± μ	H$_2$O ppm	S.D. (2σ)	F ppm	S.D. (2σ)	S ppm	S.D. (2σ)	Cl ppm	S.D. (2σ)
0 core	6	29.22	4.38	8.58	0.86	262.4	26.2	0.274	0.027
15	6	28.15	4.22	8.52	0.85	261.2	26.1	0.261	0.026
30	6	26.75	4.01	8.40	0.84	259.8	26.0	0.261	0.026
45	6	25.62	3.84	8.31	0.83	263.3	26.3	0.264	0.026
60	6	23.02	3.45	7.97	0.80	260.1	26.0	0.259	0.026
75	6	21.06	3.16	7.62	0.76	255.7	25.6	0.244	0.024
90	6	18.93	2.84	7.00	0.70	237.2	23.7	0.219	0.022
105	6	16.23	2.43	6.14	0.61	218.4	21.8	0.192	0.019
120	6	13.69	2.05	5.21	0.52	216.3	21.6	0.140	0.014

Supplementary Information Table 5: Model Parameters for the Diffusion from a Sphere with Concomitant Surface Evaporation
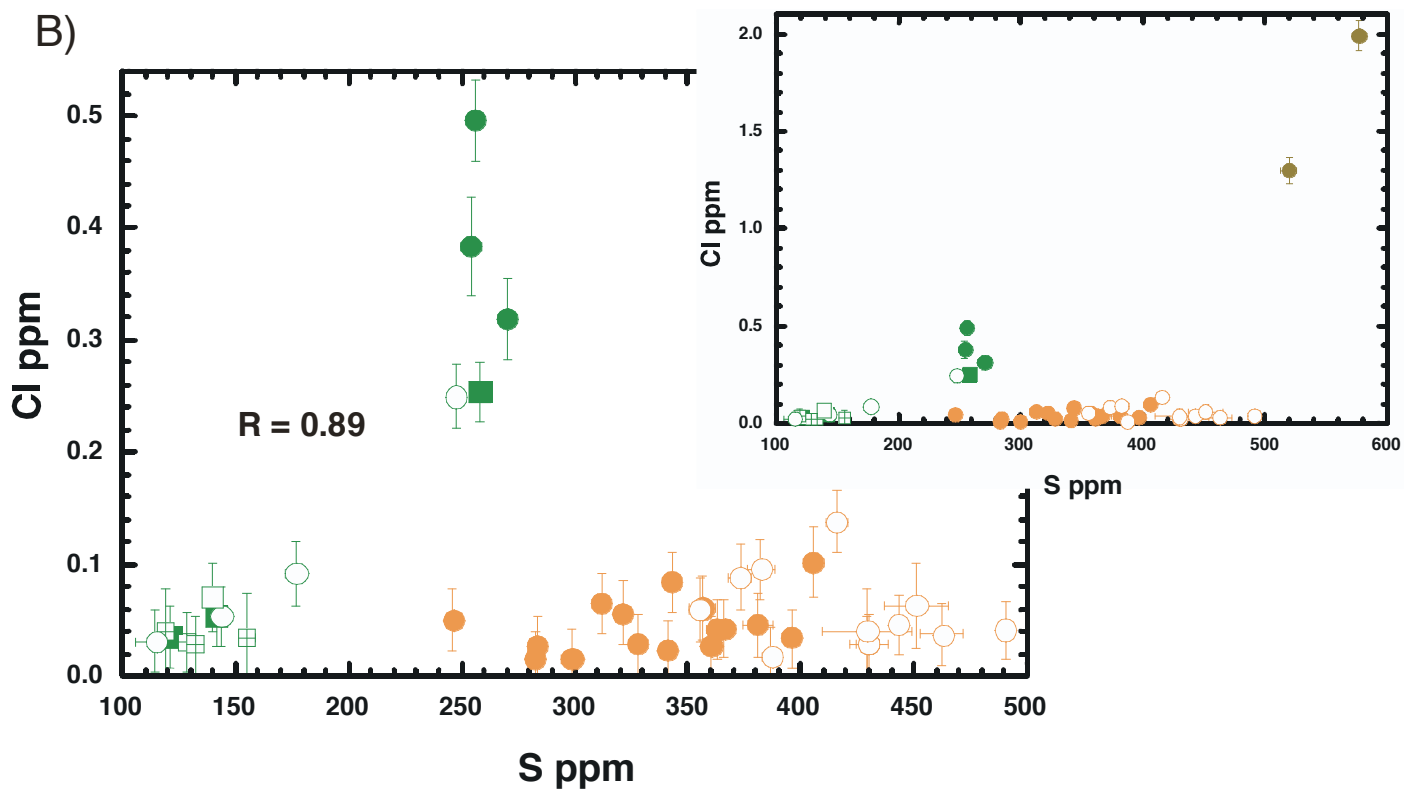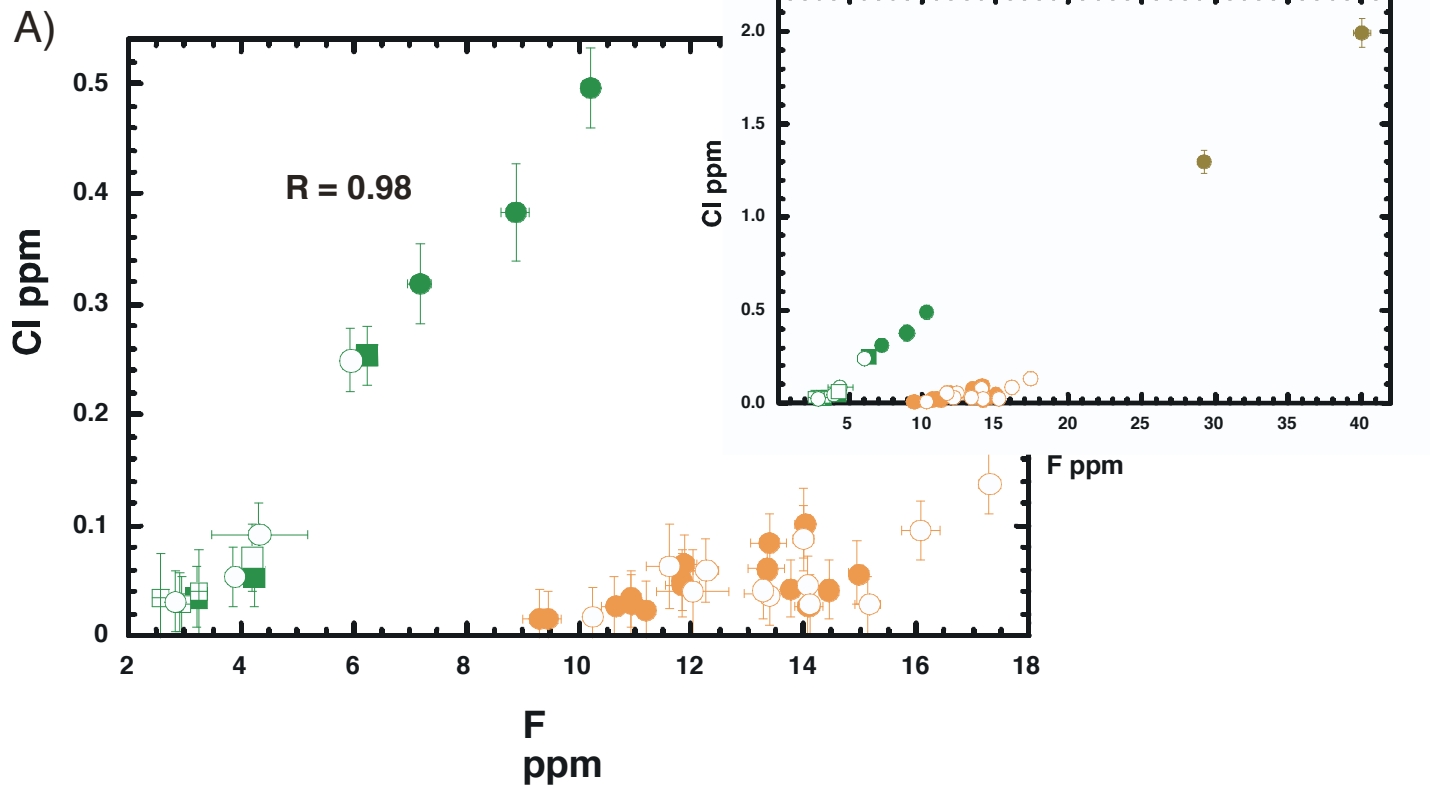
Case 1	Do (m²/sec)	E (Jouls)	D at 1450 °C (m²/sec)	Initial concentrations (ppm)	Glass bead radius (µm)	rate of evaporation (a; m/sec)[37]	Cooling Rates (°C/sec)7	Time to quench (sec)	Reference
CO_2	3.50E-04	195000	4.29E-10	ND	138	ND	-2	300	1; 2
H_2O	3.80E-06	126000	5.75E-10	745	138	7.05E-07	-2	300	2
Cl	3.40E-04	207000	1.80E-10	0.395	138	1.70E-07	-2	300	3
F	5.60E-06	159000	8.47E-11	10.7	138	1.13E-07	-2	300	4
S	9.10E-05	215000	2.76E-11	263	138	4.20E-08	-2	300	5;6;7

Case 2	Do (m²/sec)	E (Jouls)	D at 1450 °C (m²/sec)	Initial concentrations (ppm)	Glass bead radius (µm)	rate of evaporation (α; m/sec)[37]	Cooling Rates (°C/sec)7	Time to quench (sec)	Reference
CO_2	3.50E-04	195000	4.29E-10	ND	138	ND	-3	120	1; 2
H_2O	3.80E-06	126000	5.75E-10	1050	138	2.04E-06	-3	120	2
Cl	3.40E-04	207000	1.80E-10	0.405	138	4.06E-07	-3	120	3
F	5.60E-06	159000	8.47E-11	10.35	138	2.60E-07	-3	120	4
S	9.10E-05	215000	2.76E-11	260	138	8.00E-08	-3	120	5;6;7

1. Watson et al 1982[49]
2. Zhang and Stolper 1991[50]
3. Watson and Bender 1980[51]
4. Dingwell and Scarfe 1984[52]
5. Delano et al. 1994[36]
6. Wendlandt 1991[40]
7. Baker and Rutherford 1996[41]

Average Trace Element Composition of Lunar Volcanic Glasses

Legend:
- Very-low-Ti glass (B-C)
- Very-low-Ti glass (A-D)
- High-Ti glass
- Low-Ti glass

Y-axis: Trace Element/PM

X-axis: Ba Nb K La Ce Pr Sr Nd Zr Hf Sm Eu Ti Gd Tb Dy Y Ho Er Tm Yb Lu
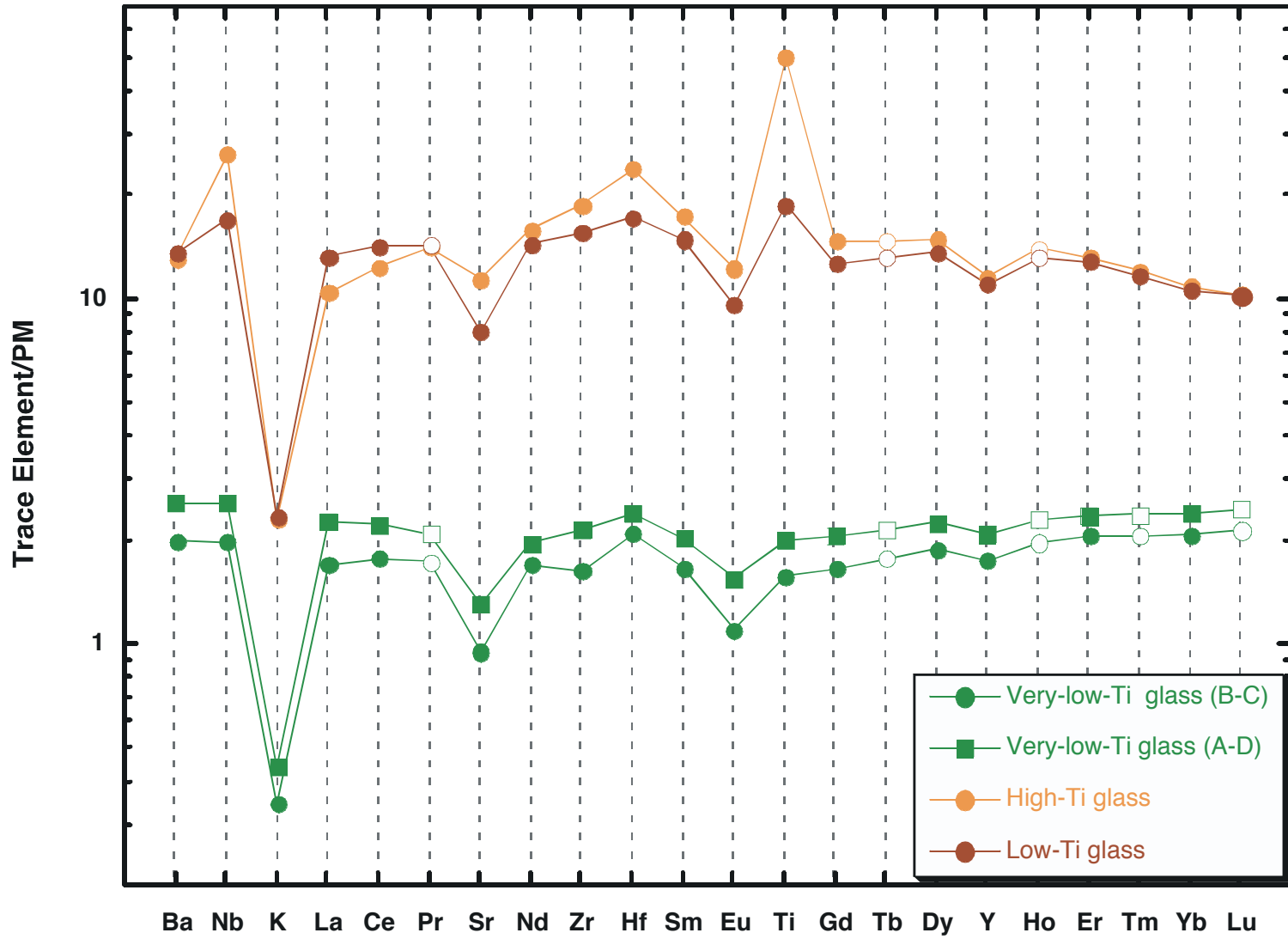
Supplementary Information Figure 1

A) R = 0.98

B) R = 0.89

C)

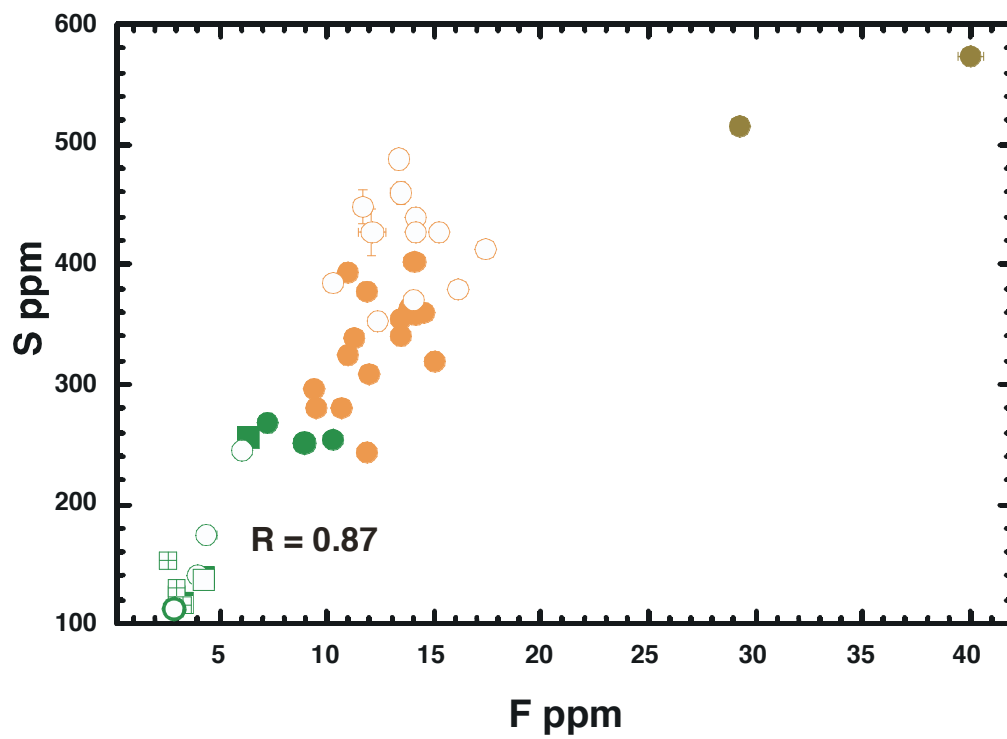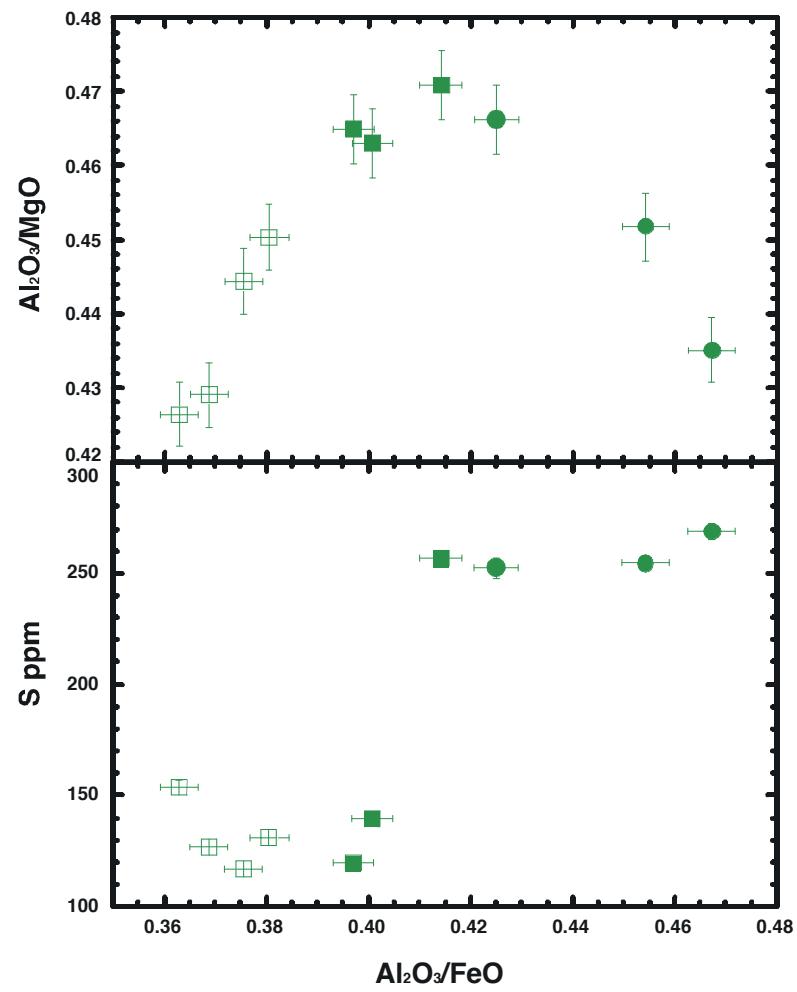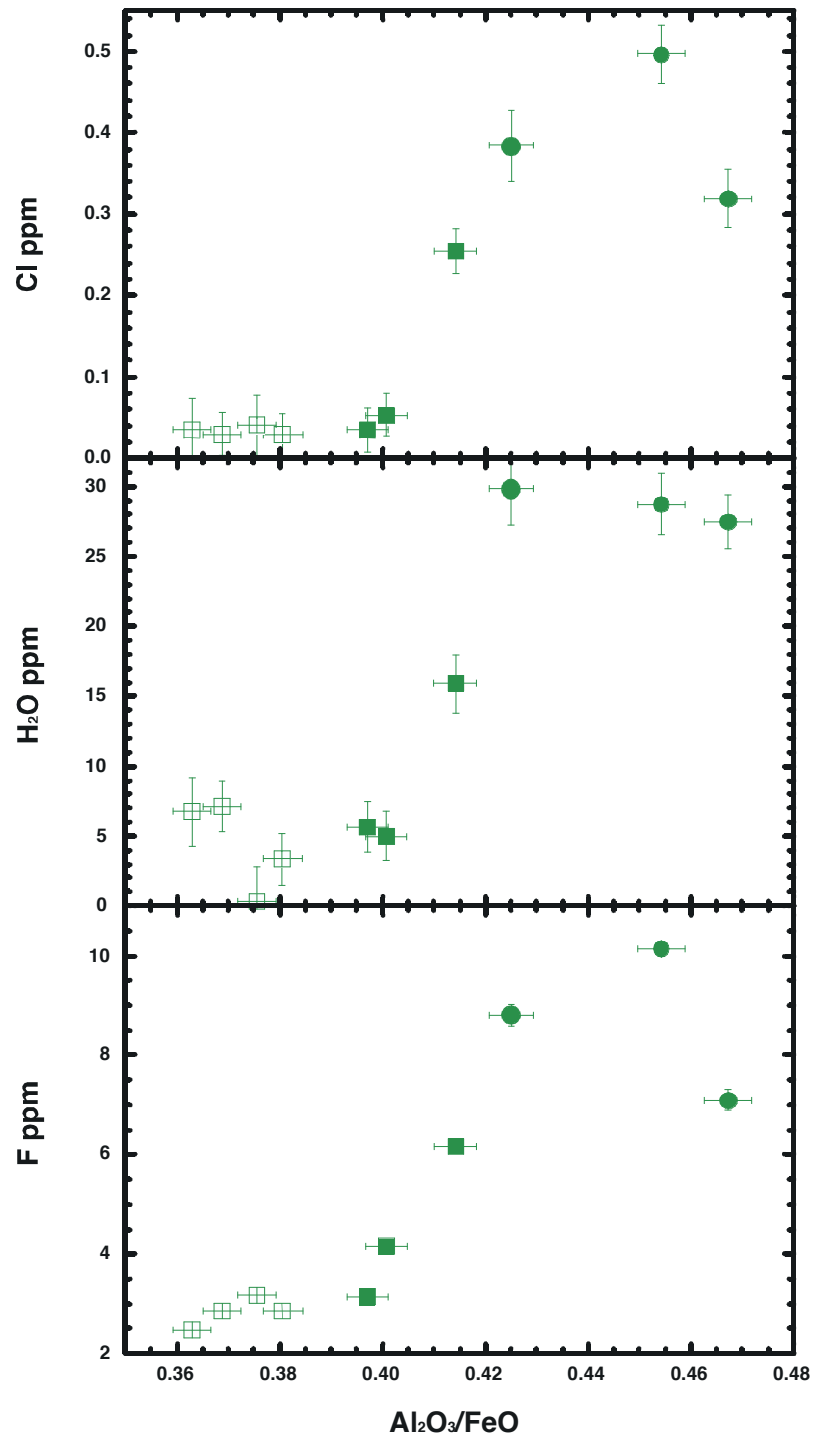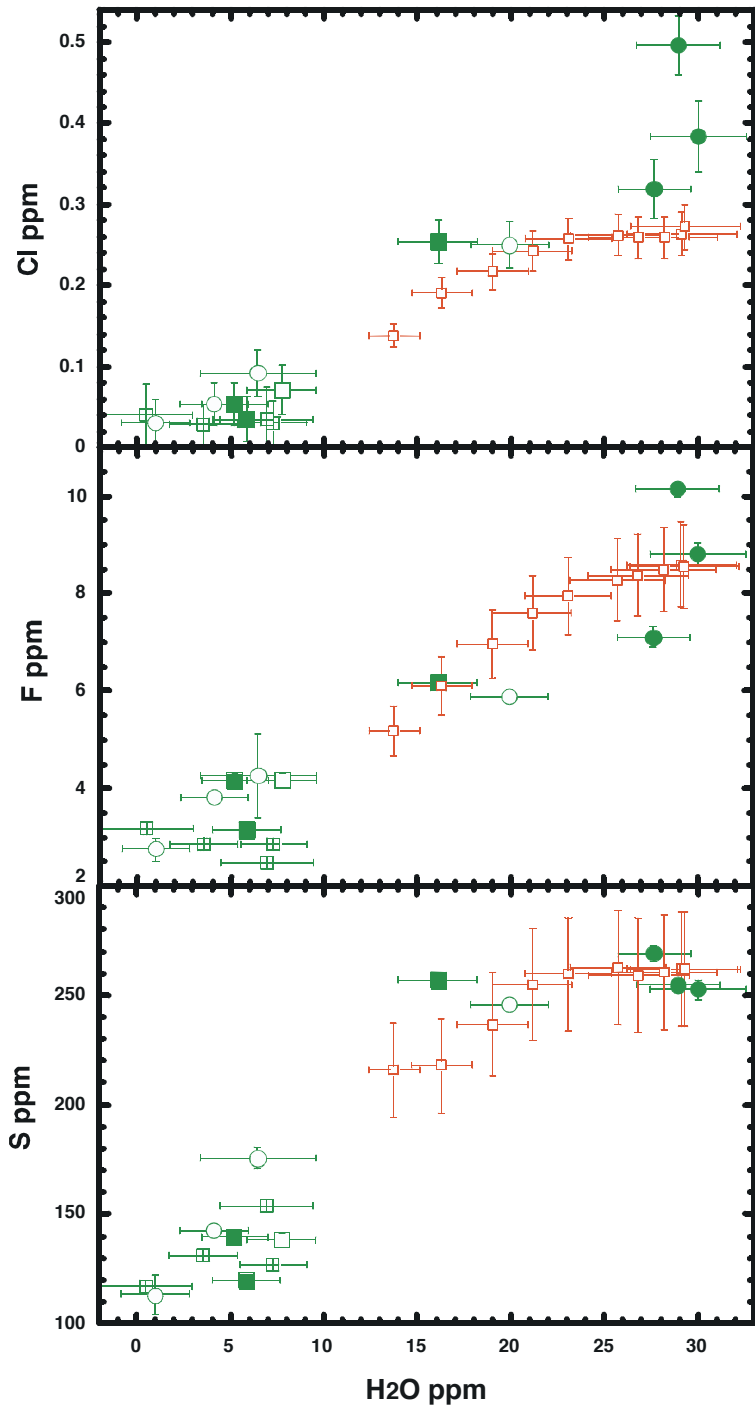R = 0.87

Supplementary Information Figure 2

Saal-2007-10-10405B
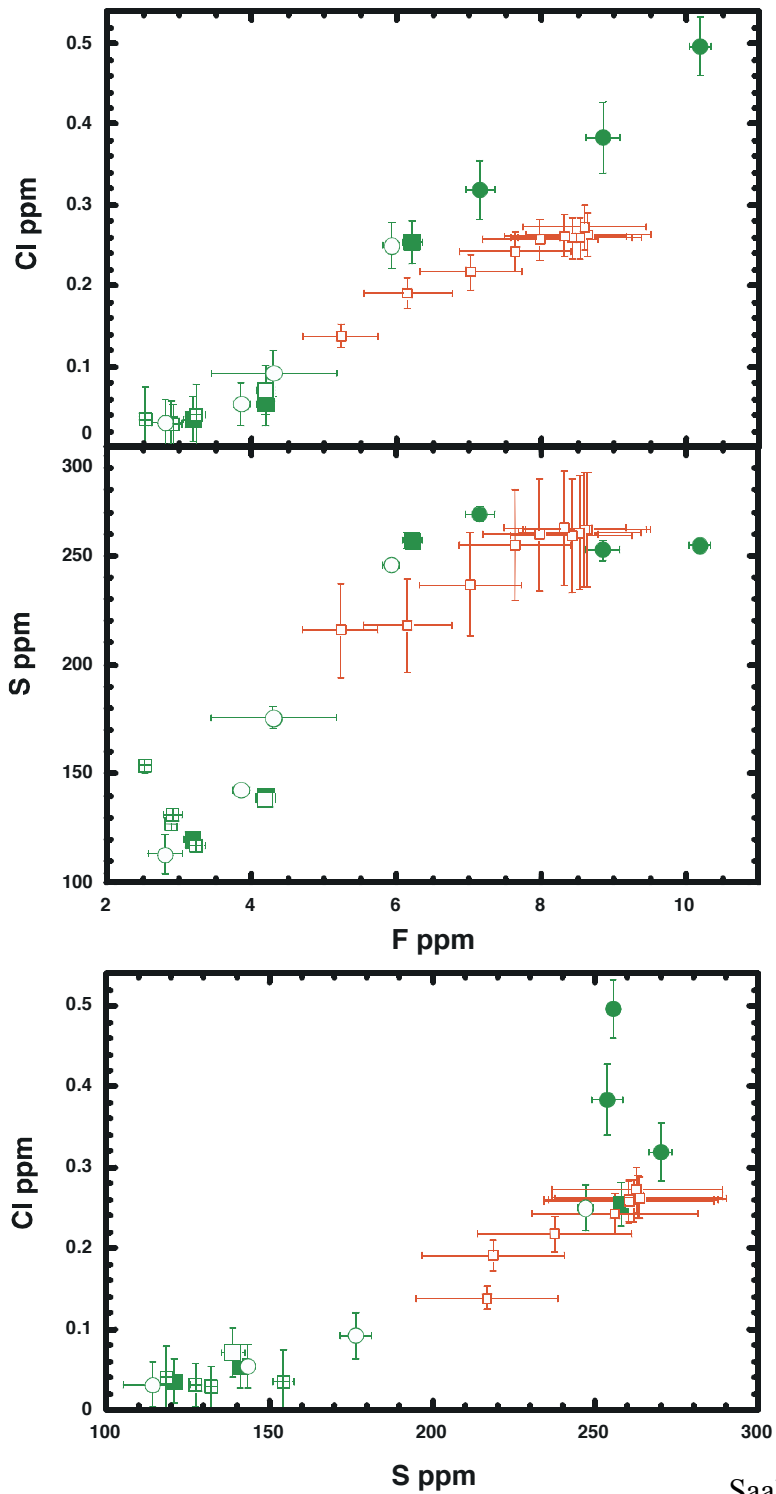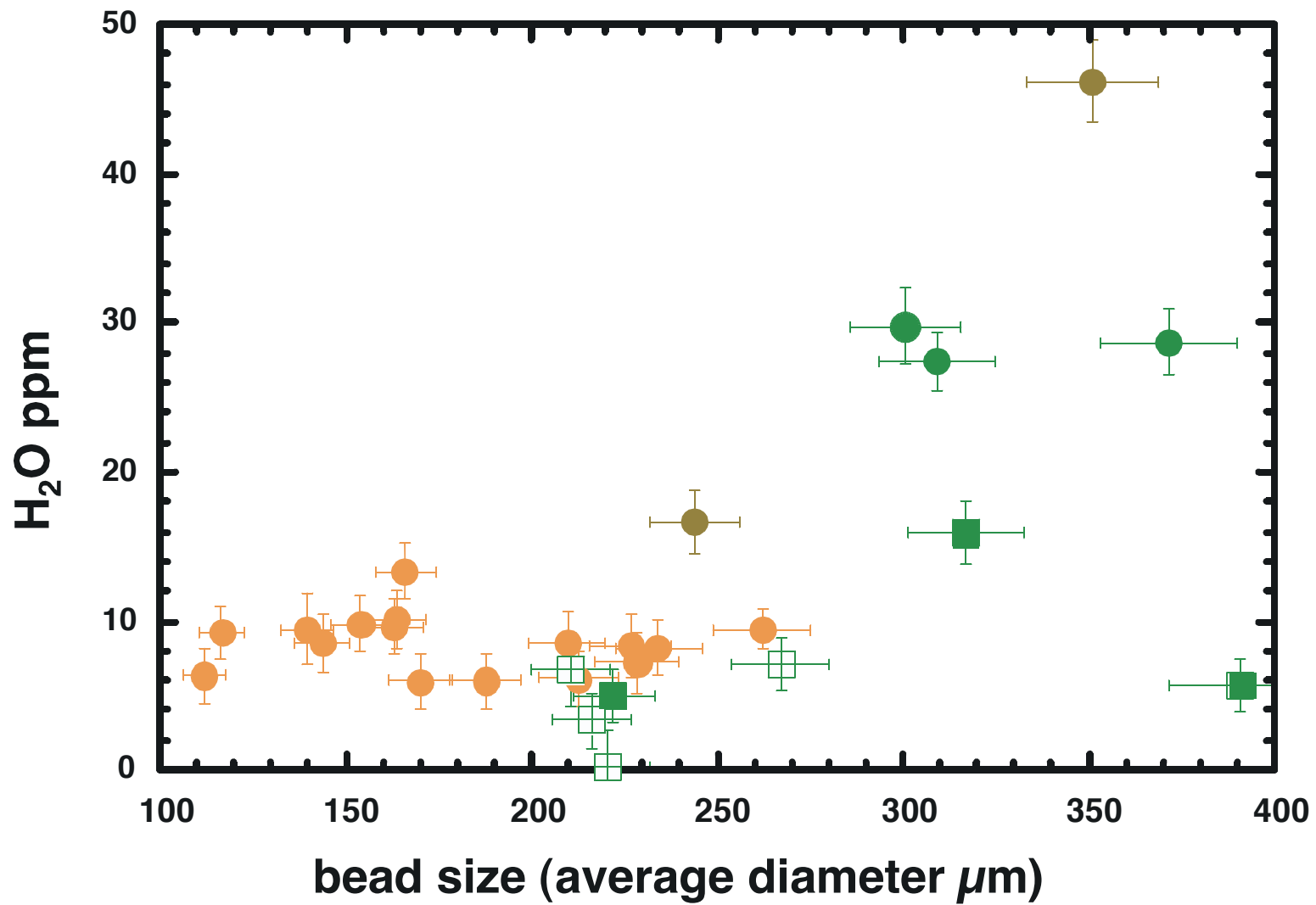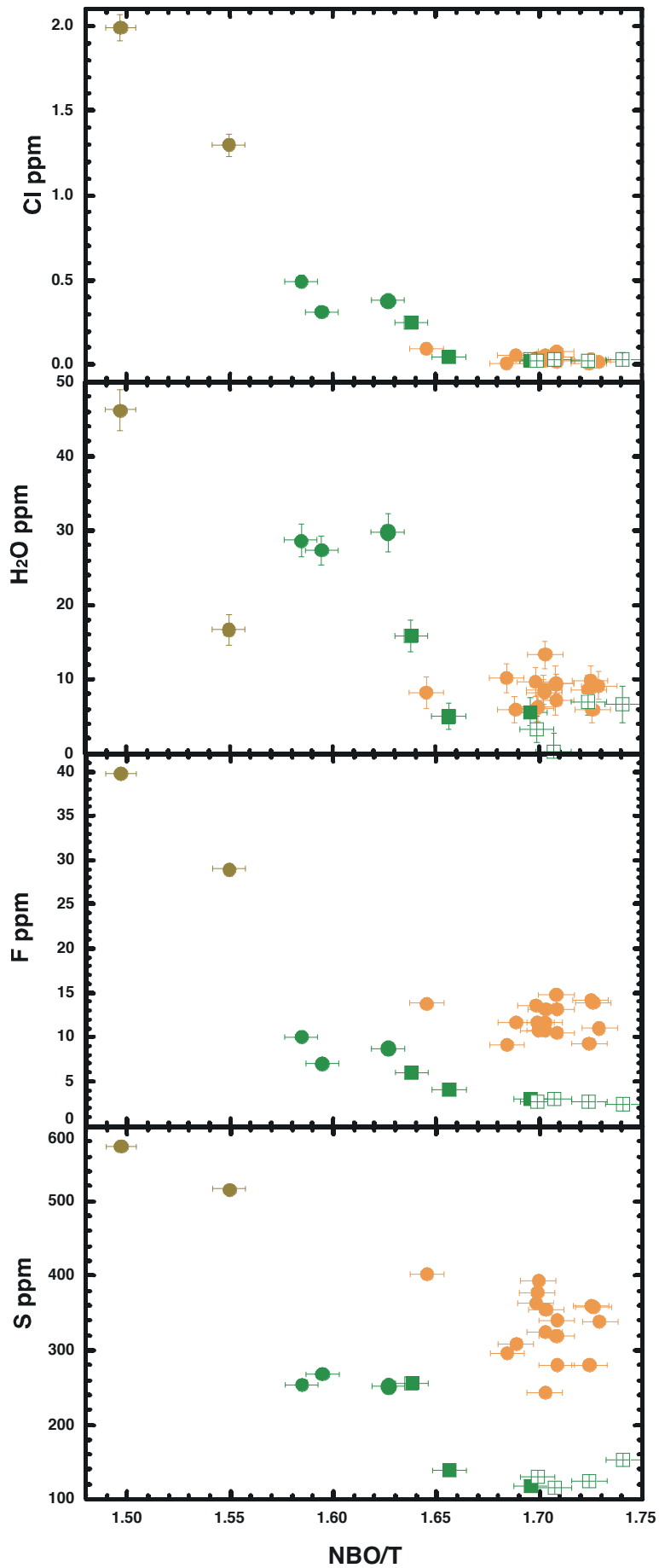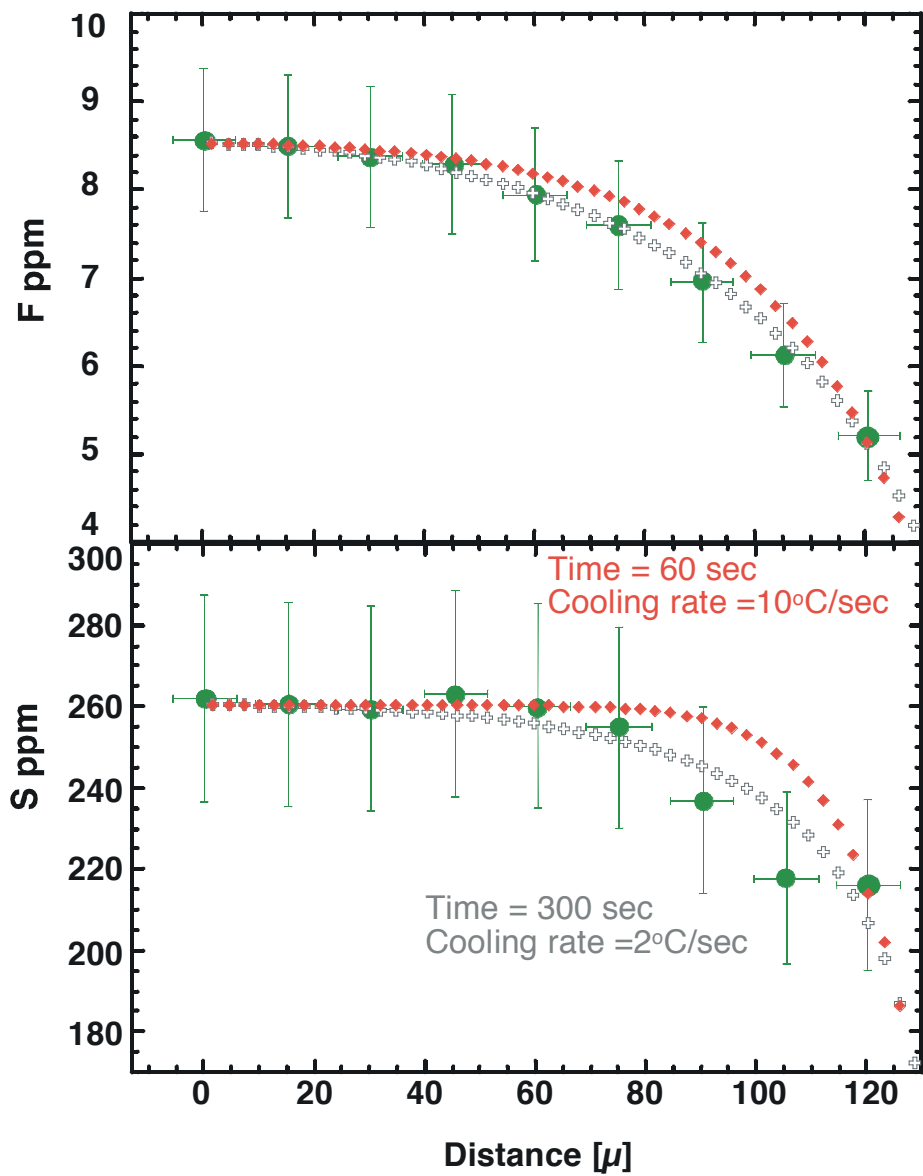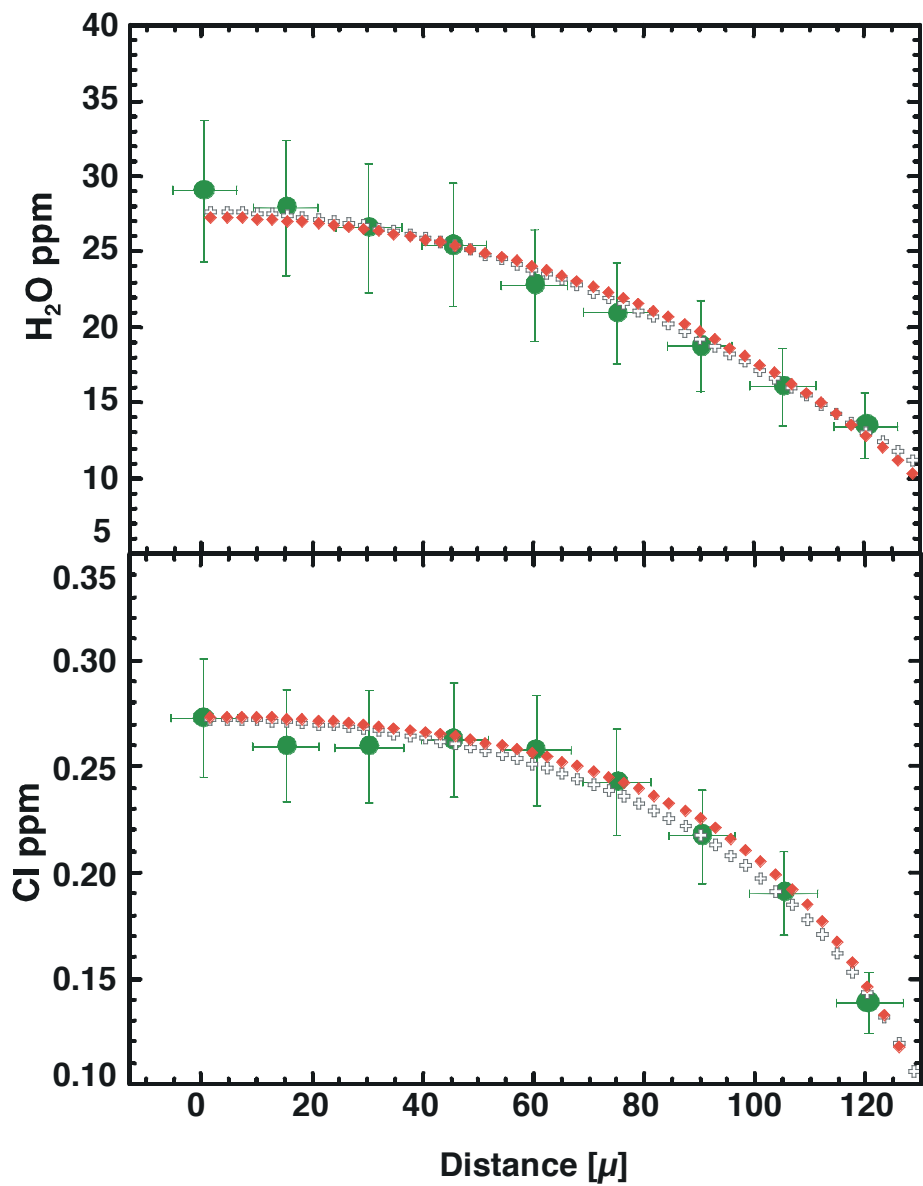
Supplementary Information Figure 3

Supplementary Information Figure 4

Supplementary Information Figure 7